Scrutinising the isolated and combined effects of in-service temperature and moisture on mode I fatigue delamination of CFRPs

Monticeli, Francisco Maciel; Biagini, Davide; Pascoe, John Alan; Mosleh, Yasmine

DOI
10.1016/j.compositesb.2025.113366

Licence
CC BY

Publication date
2026

Document Version
Final published version

Published in
Composites Part B: Engineering

Citation (APA)
Monticeli, F. M., Biagini, D., Pascoe, J. A., & Mosleh, Y. (2026). Scrutinising the isolated and combined effects of in-service temperature and moisture on mode I fatigue delamination of CFRPs. *Composites Part B: Engineering*, *313*, Article 113366. https://doi.org/10.1016/j.compositesb.2025.113366

Composites Part B 313 (2026) 113366

Contents lists available at ScienceDirect

Composites Part B

journal homepage: www.elsevier.com/locate/compositesb

Scrutinising the isolated and combined effects of *in-service* temperature and moisture on mode I fatigue delamination of CFRPs

Francisco Maciel Monticeli [a,*], Davide Biagini [a], John-Alan Pascoe [a], Yasmine Mosleh [b]

[a] Department of Aerospace Structures and Materials, Faculty of Aerospace Engineering, Delft University of Technology, Kluyverweg 1, 2629 HS, Delft, the Netherlands
[b] Department of Engineering Structures, Faculty of Civil Engineering and Geosciences, Delft University of Technology, Stevinweg 1, 2628 CN, Delft, the Netherlands

ARTICLE INFO

Keywords:
CFRP/Epoxy
Environmental effects
Fatigue
Hygrothermal conditioning

ABSTRACT

Given the long-term use of carbon fibre reinforced polymers (CFRP) in harsh environments, this study investigates the isolated and combined effects of temperature and moisture variations on mode I fatigue delamination propagation. Several levels of temperature and relative humidity were applied as preconditioning and as *in-service* during fatigue testing to evaluate their effects on the Paris curve. In addition, statistical analyses, including analysis of variance (ANOVA), semi-empirical interpolation modelling, and fractographic assessments, were conducted to provide a comprehensive understanding of the failure mechanisms. The results indicate that the moisture absorbed during hygrothermal preconditioning and the *in-service* temperature applied during fatigue test individually affect the Paris curve slope. These factors interact synergistically, significantly altering the fatigue crack growth rate. An empirical model capturing this interaction showed good agreement with experimental data, enabling reliable prediction of environmental degradation trends. Fractographic evidence supported the observed changes in fracture patterns, linking changes in fibre bridging formation, surface roughness, and energy dissipation to the observed shifts in fatigue behaviour.

1. Introduction

Driven by their high stiffness-to-weight ratio and superior mechanical performance, carbon fibre reinforced polymers (CFRPs) have been increasingly applied in various industrial sectors, including aerospace [1], automotive [2], wind energy [3,4], and in the oil and gas industry for pipeline reinforcement [5]. Their application in extreme environments, such as offshore structures, high altitude aerospace components and renewable energy systems, highlights the growing demand for lightweight, high performance materials capable of withstanding harsh operating environments [3,6,7].

Despite their advantages, CFRP components are highly susceptible to environmental degradation due to the nature of their polymer matrix [8]. Factors such as temperature, humidity, ultraviolet (UV) radiation and chemical ageing can significantly alter their mechanical properties [9,10]. In particular, thermal cycling can cause microcracking and residual stresses due to differences in the coefficient of thermal expansion (CTE) between the matrix and the fibres [11,12]. Similarly, moisture absorption leads to plasticisation, swelling and potential hydrolytic degradation, further compromising mechanical performance and durability [13,14]. As structural components are subjected to cyclic loading in harsh operational environments, understanding the damage evolution in combination with environmental factors—particularly delamination growth under fatigue — becomes crucial for ensuring long-term performance and structural integrity.

Given the inherently weak interlaminar interface in composite laminates [15], the introduction of environmental effects adds an additional layer of complexity to the failure mechanisms involved. This is because external environmental parameters such as temperature and humidity can alter the behaviour at both micro and meso scale, which is captured through characterisation curves at the coupon level [16,17], thus requiring a greater amount of testing for characterisation and/or certification. As industries continue to push the operational boundaries of CFRP-based structures, the reliable assessment of damage initiation and progression under fatigue loading becomes ever more important. This issue becomes critical for ensuring structural integrity, improving fatigue life prediction, and supporting the broader adoption of CFRPs in applications exposed to environmental conditions [18–20].

Changes in the physical and thermo-mechanical properties of polymer matrix composites caused by environmental conditions, such as

* Corresponding author.
E-mail addresses: f.m.monticeli@tudelft.nl, francisco.monticelli@gmail.com (F.M. Monticeli), D.Biagini-1@tudelft.nl (D. Biagini), J.A.Pascoe@tudelft.nl (J.-A. Pascoe), Y.Mosleh@tudelft.nl (Y. Mosleh).

https://doi.org/10.1016/j.compositesb.2025.113366
Received 23 September 2025; Received in revised form 1 December 2025; Accepted 28 December 2025
Available online 29 December 2025

temperature and moisture, pose a significant challenge to structural integrity and design. These effects are particularly pronounced on the fracture toughness and fatigue resistance of bonded and laminated interfaces [16,17]. Consequently, several studies have proposed numerical and semi-empirical approaches to modelling and predicting degradation mechanisms under environmental conditions. For example, numerical modelling (Cohesive Zone Modelling - CZM) has been employed to predict the effect of temperature on delamination in individual modes I and II [21,22]. In these models, temperature-dependent elastic properties were obtained from experiments, to account for the effect of temperature [21]. Similarly, Landry et al. [22] applied CZM to simulate the effects of exposure to water, hydraulic fluid, and de-icing fluid on mode II fatigue delamination, using material properties experimentally obtained for each conditioning scenario.

Charalambous et al. [23] proposed a semi-empirical solution, where the slope of the Paris curve (n) becomes a function of the normalised temperature $n(T) = n_0(T/T_0)^{\gamma}$, where n_0 and γ are material constants and T_0 is a reference temperature. The results showed a good correlation with the experimental curves. Furthermore, Yao et al. [24] conducted a comprehensive investigation on the influence of temperature on mode I fatigue delamination behaviour, employing the normalised strain energy release rate (SERR) as a similitude parameter to evaluate the intrinsic fatigue delamination resistance. In their approach, both the shift in the SERR (at a fixed crack growth rate, da/dN) and the variation in the slope (n) of the intrinsic resistance curve were analysed. These effects were quantitatively modelled through a second-order polynomial interpolation as a function of the applied operational temperature, yielding good agreement with the experimental data.

Regarding the hygrothermal ageing effect, Yao et al. [25] employed both the modified Paris relation $\frac{da}{dN} = C\left[\frac{G_{IC0}}{G_{IC}(a-a_0)}\Delta\sqrt{G}\right]^n$ and a two-parameter Paris-type formulation $\frac{da}{dN} = C\left[\Delta\sqrt{G_{tip}}\left[1-\left(\frac{G_{\max\_tip}}{G_{IC0}}\right)^{\gamma}\right]G_{\max\_tip}\left(\frac{G_{\max\_tip}}{G_{IC0}}\right)\right]^n$ to characterise the intrinsic fatigue delamination resistance at the crack front—that is, delamination behaviour excluding the retardation effects induced by fibre bridging. For each equation, G_{IC0} is fatigue resistance excluding fibre bridging contribution, G_{IC} is the fracture toughness at a given pre-crack length ($a - a_0$), $\Delta\sqrt{G} = (\Delta\sqrt{G_{max}} - \Delta\sqrt{G_{min}})^2$, $\Delta\sqrt{G_{tip}}$ is the SERR range around delamination front, G_{max_tip} represents the maximum SERR around delamination front, γ is the weight-parameter, da/dN is the crack grow rate and C and n are fitting parameters. Their study provides clear evidence that both Paris-type formulations can accurately describe fatigue delamination propagation, with strong experimental validation under various ageing conditions [17] as well as for different fibre orientations exposed to hygrothermal environments [16].

The temperature has either an accelerating or retarding effect on delamination behaviour and influences the underlying micro mechanisms of failure, with these effects being highly dependent on exposure time [23]. On the other hand, Ramirez et al. [26] carried out an analysis of the hygrothermal effects (control of temperature and relative humidity – RH) on fatigue delamination under mode I and mode II loading, highlighting the role of plasticisation at the fracture surfaces, which in turn leads to an increase in material toughness. A similar investigation into the effects of hygrothermal ageing on Mode I fatigue delamination was conducted using samples preconditioned in a climatic chamber before the test [25]. The results demonstrated that temperature variations affect the glass transition temperature (T_g), which in turn significantly affects the SERR and alters fatigue crack growth behaviour as described by the Paris equation. However, in real-world applications, structural components are subjected to cyclic loading while simultaneously experiencing *in-situ* hygrothermal exposure. This poses a significant challenge, as the application of temperature without proper humidity control during fatigue testing can lead to moisture loss, partially restoring the original mechanical response of the material [17]. It is therefore essential to characterise not only the isolated effects of temperature and prior hygrothermal conditioning, but also those that arise under *in-service* cyclic loading, to accurately capture the degradation induced by environmental exposure. A key question is how individual hygrothermal parameters alter Mode I fatigue delamination, particularly in terms of fracture toughness and crack propagation behaviour. Furthermore, for structural components operating under *in-service* environments, it is crucial to understand the combined effects of preconditioning (ageing) and *in-service* temperature and relative humidity (RH) on fatigue delamination.

In order to address the aforementioned research questions, this study investigated the effect of in-service moisture and temperature conditions, both individually and in combination, on mode I fatigue delamination behaviour. The study focused on elucidating changes in the Paris curve parameters. To this end, CFRP specimens were subjected to different precondition levels (temperature and relative humidity) to isolate and quantify their individual and combined effect of hygrothermal ageing on mode I fatigue delamination. In addition, a comprehensive analysis of failure mechanisms and their contribution to fatigue crack growth behaviour was conducted through statistical analyses using analysis of variance (ANOVA), semi-empirical interpolation modelling and fractographic assessments.

2. Materials and methods

Unidirectional (UD) carbon fibre IM7 pre-impregnated with epoxy resin 8552 from Hexcel® was used to manufacture the composite laminates, consisting of 24 plies, arranged in a $[0]_{24}$ stacking sequence. The curing process was performed in an autoclave at 120 °C for 2 h, followed by a second hold at 180 °C for 4 h, under a vacuum of 0.2 bar and a pressure of 7 bar throughout the process.

The elastic properties of the unidirectional lamina are presented in Table 1, based on manufacturer data and supported by relevant literature sources [27–29].

2.1. Environmental conditioning

Given the complexity of the combinations of environmental conditions applied prior to or during mechanical testing, some key terms used throughout this paper are defined for clarity and consistency:

- Pristine samples (dry): Specimens that were tested without any prior hygrothermal preconditioning are referred to as pristine samples. These specimens are considered as reference of minimal water content (0 wt%).
- Preconditioned samples (wet): Specimens that were preconditioned in climatic chambers under controlled temperature and relative humidity prior to mechanical testing, allowing them to reach a specified level of moisture absorption (>0.00 wt%).

Hygrothermal preconditioning refers to the prior exposure of the specimen in a climatic chamber. After specimen cutting, the samples were placed in a Weiss Environmental Chamber 0830 at different combinations of temperature and humidity according to the standardised procedures of ASTM D5229 [30]. The samples were weighed at intervals of 2–5 days to assess the change in mass, which in this case refers to the moisture absorption that changes the specimen mass over time.

The moisture content (based on normalised mass measurement – Eq. (1)) was measured during preconditioning until reaching the equilibrium moisture content (EMC), which is defined as the moisture level at which a material no longer absorbs or desorbs water when exposed to a constant temperature and relative humidity. At this point, the rate of moisture absorption equals the rate of desorption, resulting in a stable

Table 1
IM7/8552 UD lamina properties [27–29].

E_{11} (GPa)	E_{22} (GPa)	G_{12} (GPa)	G_{23} (GPa)	ν_{12}= ν_{13}	ν_{23}	*TGA* (°C)	Density (g/m^3)	σ_{1t} (MPa)
161	11.38	5.17	3.98	0.32	0.43	340	1.56	3310

internal moisture content. This state is considered representative of the material's long-term moisture uptake under given environmental conditions and is crucial for evaluating hygrothermal effects on mechanical properties for each level of hygrothermal conditions. The EMC is given by the following equation:

$$EMC(\%) = \frac{m_f - m_i}{m_i} \times 100 \quad (1)$$

where *EMC* is the equilibrium moisture content (in weight %), m_i is the initial mass of the sample and m_f is the final mass of the sample after a certain duration of hygrothermal exposure.

Fig. 1 shows the three main levels of hygrothermal preconditioning conducted in the climatic chamber. The curve shows the change of normalised mass due to moisture absorption. The colour shadings represent different levels of relative humidity set during conditioning, while the temperature was maintained at 90 °C. Level (I) refers to samples without any level of preconditioning in a climate chamber (dry samples). The red-shaded region represents the period of maximum moisture exposure (90 % relative humidity), during which the material reached near-equilibrium saturation after 60 days. The moisture saturation is confirmed by the stabilisation of mass gain in repeated measurements. This plateau in moisture uptake is also consistent with values and time reported in the literature for similar CFRP laminates [31].

This condition is defined as Level II, with an average moisture uptake of 1.20 wt%. The blue-shaded region corresponds to Level III, where the relative humidity was reduced to 50 %, while the temperature was maintained at 90 °C, leading to moisture desorption. This resulted in an average decrease in moisture uptake to 0.85 wt%. In the green-shaded region, the relative humidity was further reduced to 30 % at 90 °C, leading to a new conditioning stage — Level IV — characterised by an average equilibrium moisture content of around 0.55 wt%.

After reaching the equilibrium moisture content (EMC) defined for each conditioning level (see Fig. 1), the specimens underwent fatigue testing in a climatic chamber integrated with a fatigue machine (see Fig. 2). To ensure consistency, the temperature and relative humidity during testing were matched to those used in the hygrothermal preconditioning phase.

The target temperature and humidity were maintained throughout the fatigue tests by actively controlling the environmental conditions within the chamber, particularly for wet specimens. This preserved the hygrothermal saturation state achieved during preconditioning during cyclic loading. This testing approach was applied to both dry and wet specimens. The detailed procedure for mode I fatigue delamination testing under cyclic loading is presented in the following section.

To evaluate the isolated effects of hygrothermal conditions, the tests were divided into groups with different combinations of temperature and relative humidity. *In-service* environmental conditioning during fatigue test refers to the application of controlled temperature and relative humidity during mechanical testing using a Weiss Technik 600C climatic chamber coupled to the fatigue machine. The different temperature and moisture levels are summarised in Table 2. The first five group of tests consisted in carrying out fatigue tests on dry samples (0.00 wt% EMC) under the same combination of *in-service* temperature and relative humidity used for preconditioning samples to isolate the in-service temperature and relative humidity effect. The purpose was to generate the corresponding Paris curves and to evaluate the difference in terms of hygrothermal preconditioning, versus *in-service* hygrothermal conditioning during the test. The second group were wet conditions based on the previously discussed moisture saturation level, in order to maintain a similar level of water absorption during between preconditioning and *in-service* exposure during fatigue loading.

Three independent replicates were performed for each environmental condition under cyclic Mode I delamination testing, ensuring repeatability and statistical reliability of the Paris curve characterisation. It should be noted that the dry specimens tested under elevated temperature (80 °C) and variable relative humidity conditions (90, 50 and 30 % RH) were not exposed for long enough to absorb measurable amounts of moisture. Nevertheless, these tests were necessary in order to statistically define the lower and upper limits of the EMC range. Additionally, due to limitations of the in-situ climatic chamber integrated with the fatigue test system, which does not permit simultaneous application of high temperature and high humidity, specimens preconditioned at 90 °C were tested at 80 °C.

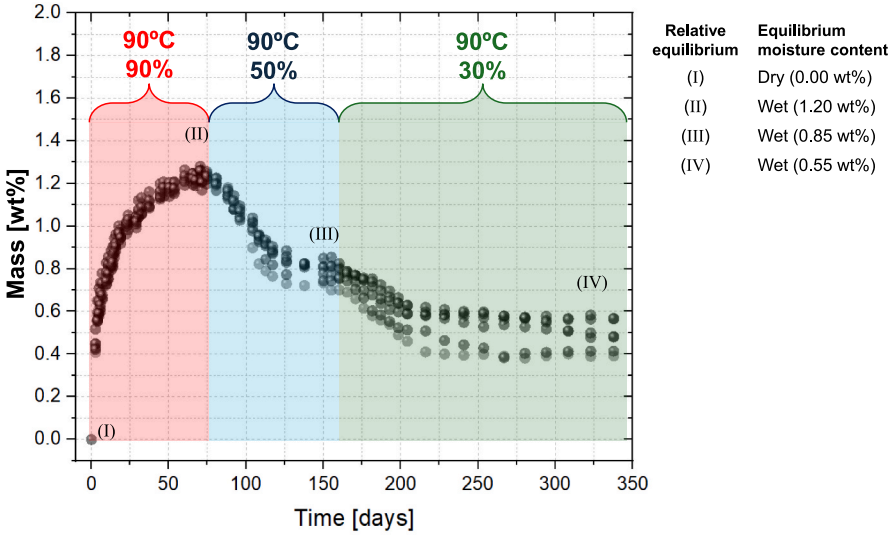

Fig. 1. Experimental moisture absorption progression of IM7/8552 composites indicating levels of moisture saturation at various environmental conditions.

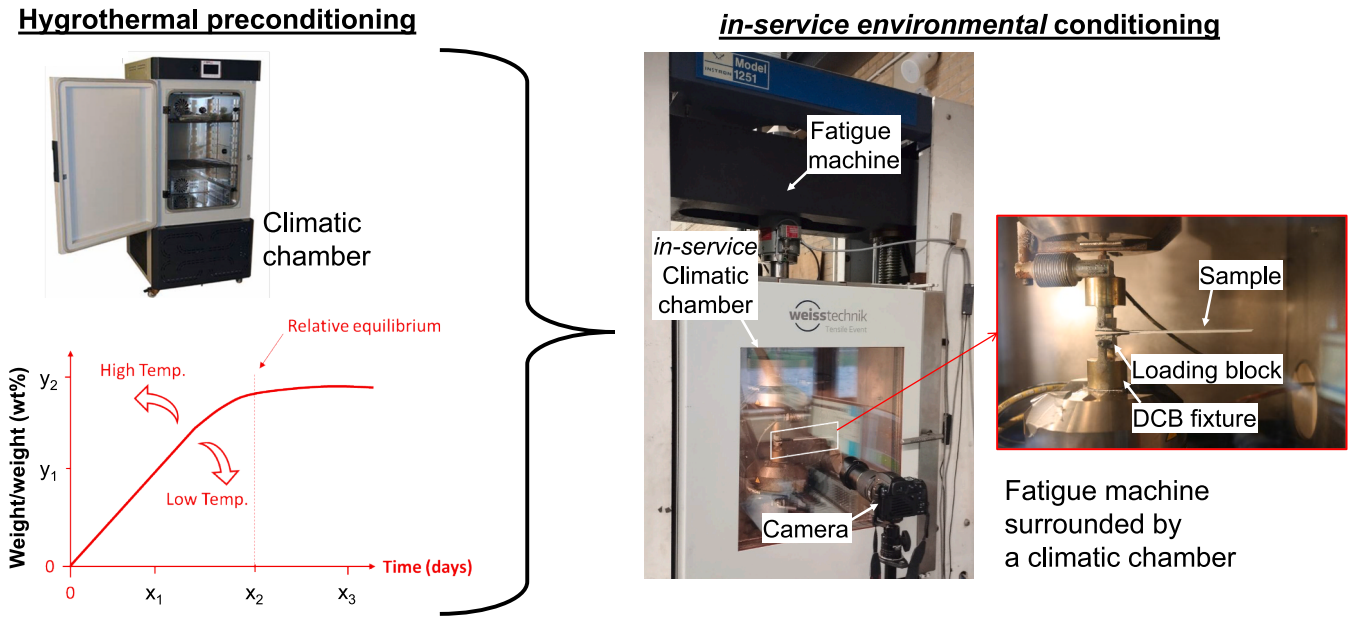

Fig. 2. A Schematic of hygrothermal mode I fatigue testing preconditioning process and *in-service* environmental conditioning.

Table 2
Overview of moisture saturation levels during *in-service* and hygrothermal pre-conditioning before and during fatigue test.

Hygrothermal preconditioning level[a] (climatic chamber)	Equilibrium moisture content	Level in Fig. 1	*in-service* environmental conditions[a] (during fatigue test)
None	Dry (0.00 wt%)	I	−40 °C
None	Dry (0.00 wt%)	I	22 °C/50 %
None	Dry (0.00 wt%)	I	[b]80 °C/90 %
None	Dry (0.00 wt%)	I	[b]80 °C/50 %
None	Dry (0.00 wt%)	I	[b]80 °C/30 %
90 °C/90 %	Wet (1.20 wt%)	II	−40 °C
90 °C/90 %	Wet (1.20 wt%)	II	22 °C/50 %
90 °C/90 %	Wet (1.20 wt%)	II	80 °C/90 %
90 °C/50 %	Wet (0.85 wt%)	III	80 °C/50 %
90 °C/30 %	Wet (0.55 wt%)	IV	80 °C/30 %

None – refers to dry sample, not expose to hygrothermal preconditioning.
[a] Level of Temperature (°C) and relative humidity (%).
[b] Tested for statistical purposes.

2.2. Mechanical testing

The specimens were cut using a diamond disc according to the standardised dimensions of ASTM D5528 [32], i.e. 160 × 25 × 3 mm^3, with a PTFE insert to provide an initial crack length of a_0 = 50 mm, measuring from the load application point to the insert tip. Bonded loading blocks were used to connect the specimen to the test fixture. Mode I fatigue tests were carried out following ASTM D6115 [33] and ASTM D5528 [34].

An MTS universal servo-hydraulic machine with a 200 N load-cell was used to load the specimens. The tests were performed under displacement-controlled conditions, with the maximum applied displacment fixed at 95 % of the maximum opening displacement (δ_{max}) obtained from the quasi-static DCB pre-cracking (3–5 mm) of each condition, which can be related to 95 % of (G_{IC}). As a result, the applied load varied depending on the stiffness of each specimen and environmental condition. Therefore, the maximum load was not pre-defined but followed the imposed displacement ratio consistently across all configurations. The remain test parameters are frequency of 2.5 Hz, and R-ratio of 0.1 ($\delta_{min}/\delta_{max}$) with a constant amplitude opening. The measurement of strain energy release rate (SERR) was based on modified compliance calibration (MCC), following Equation (2). Fatigue crack growth behaviour was characterised using the Paris curve, denoted by Equation (3), with $\Delta\sqrt{G} = \left(\sqrt{G_{max}} - \sqrt{G_{min}}\right)^2$ as the similitude parameter. The experiments were carried out in triplicate, showing good repeatability of the experimental results and ensuring a consistency in the fitted parameters of the Paris model (Eq. (3)).

The increase in the crack length was monitored through image acquisition every 250 cycles, and crack length measurements were performed via post-processing using the *ImageJ* software.

$$G_I = \frac{3P_c^2 C_c^{2/3}}{2A_1 bh}\frac{F}{N}, \text{ for } C_C = \frac{\delta_{max} - \delta_{min}}{P_{max} - P_{min}} \quad (2)$$

$$\frac{da}{dN} = C\left(\Delta\sqrt{G}\right)^n \quad (3)$$

where, G_I represents SERR (max/min), P_c represents the load, C_c is the compliance δ the opening displacement, A_1 is the slope of plot of a/h versus $C_c^{1/3}$, a is the crack length, b is the width, h is the thickness, F is a parameter that corrects for the effects of large displacement at fracture, while N is a parameter that accounts for large displacements and fracture and for stiffening of the specimen by the load blocks. Again, da/dN is the fatigue crack growth rate, C and n are material-dependent fitting parameters of Paris curve.

The da/dN method was obtained by fitting the crack-length evolution to a power-law relationship of the form $a = \alpha N^{\beta}$. Differentiating this fitted function with respect to the number of cycles N then yields the fatigue crack growth rate, da/dN.

2.3. Dynamic mechanical thermal analysis (DMTA)

DMTA was performed to evaluate the effect of absorbed moisture (during conditioning) on the viscoelastic response of the materials. The equipment used was an RSA G2 DMA with samples with dimensions of 50 × 10× 3 mm^3. Two runs were performed per sample, demonstrating concise repeatability behaviour. The thermal scan was carried out from −60 °C to 300 °C at a heating rate of 1.5 °C/min under N_2 atmosphere, according to ASTM D4065, with a frequency of 1Hz. Liquid nitrogen was used for cooling. Specimens were tested using a three-point flexure fixture. The specimens tested were (*i*) the pristine specimens (Dry 0.00 wt%), (*ii*) the preconditioned specimens (Wet 1.20 wt%), and (*iii*) the

wet and subsequently dried specimens with a residual EMC of 0.55 wt% (level IV in Fig. 1).

2.4. Fractography analysis

A 3D laser scanning confocal microscope (Keyence VK-X1000, Mechelen) was used to examine the fracture surface. The confocal

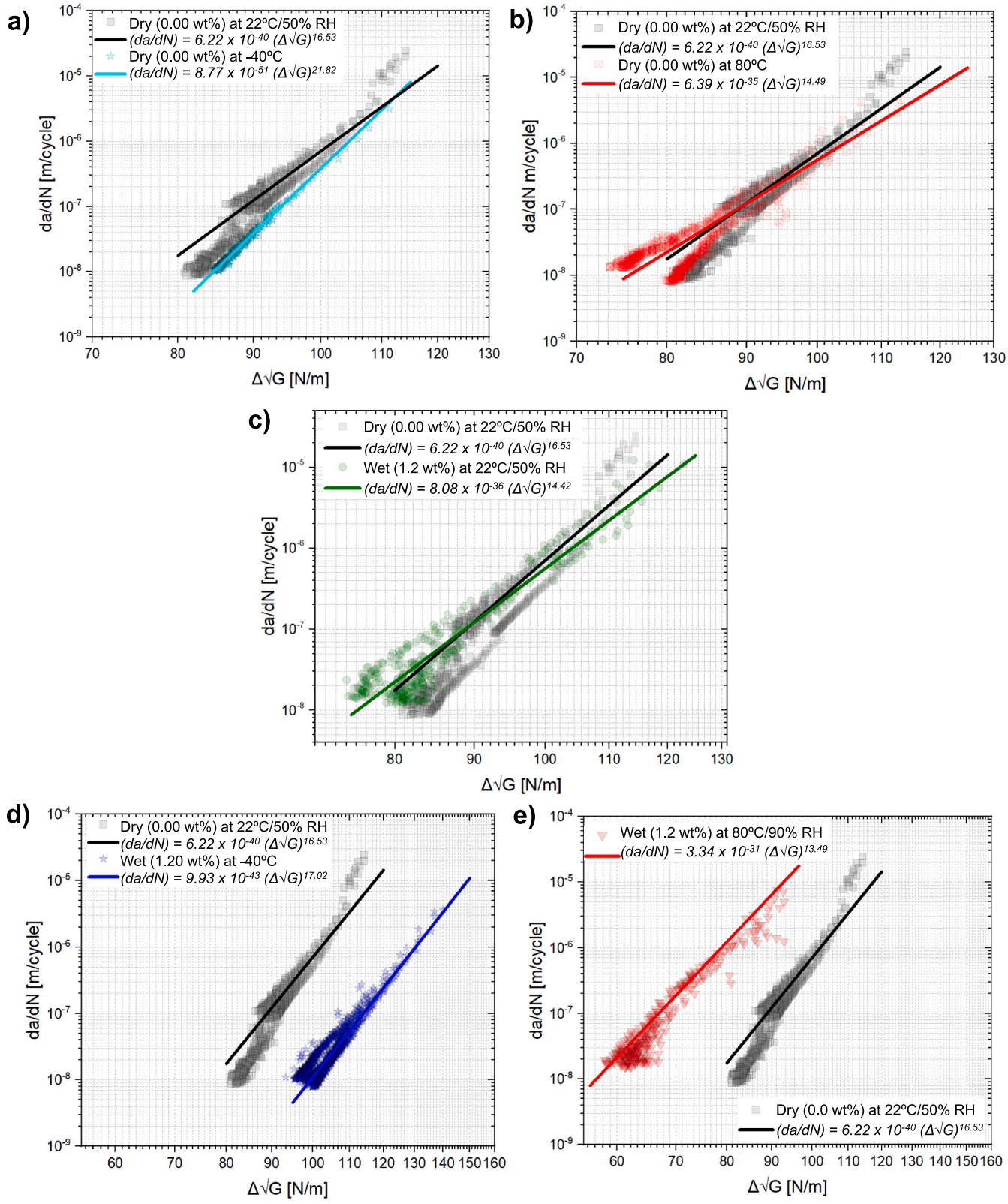

Fig. 3. Individual effect of a) *in-service* low temperature, b) *in-service* high temperature, c) hygrothermal preconditioning. Combination effect of hygrothermal preconditioning d) *in-service* high temperature (hot-wet), and d) *in-service* low temperature (low-wet).

measurement was performed to reconstruct the fracture surface in order to analyse the surface roughness according to Equation (4) following ISO 4287 and 4288.

$$R_a = \frac{1}{l}\int_0^l |y(x)|dx \quad (4)$$

where, R_a is the arithmetic mean roughness, l is sampling length, $y(x)$ is the surface profile as a function of position x (meaning the height of the surface at each point x), $|y(x)|$ is the absolute value of the surface height relative to the mean line, and $1/l$ is the normalisation factor that divides the sum of absolute height values by the total length

For additional fractographic analysis, scanning electron microscopy (SEM) was carried out. The fracture surfaces were coated with a 15 nm gold layer prior to SEM analysis. Representative specimens from each environmental conditioning group were examined to assess morphological differences. SEM images were acquired at different magnifications using an acceleration voltage of 5 keV.

3. Results and discussion

3.1. Delamination curves

In this section the Paris curves of each fatigue delamination test performed on pristine (dry) and preconditioned (wet) samples at different *in-service* environmental conditions are discussed. The full experimental data and fitting of Paris curves for each individual condition are presented in Appendix A. For each condition, three independent replicates were performed, and the resulting data exhibited strong overlap, indicating repeatability of the Paris curve parameters within each environmental configuration.

Some variability can be observed between the curves depending on the level of *in-service* conditions. To investigate this, Fig. 3 presents an analysis of the isolated effects by comparing each condition with the baseline, i.e. the pristine sample (dry 0.00 wt %) tested at room conditions and without prior conditioning (i.e. 22 °C 50 %RH). Specifically, Fig. 3a presents the isolated effect of negative *in-service* temperature (−40 °C); Fig. 3b the isolated effect of high *in-service* temperature (80 °C); Fig. 3c, the isolated effect of hygrothermal preconditioning (*wet 1.20 wt %*) in climatic chamber and tested at room conditions (22 °C/50 % RH); Fig. 3d represents the combination of precondition (*wet 1.20 wt %*) and *in-service* low temperature, i.e. low-wet condition; and Fig. 3e the combined effect of hygrothermal preconditioning (*wet 1.20 wt %*) and high *in-service* temperature (hot-wet condition). The comparison reference curve for all cases is for dry specimens, without preconditioning, and tested at 22 °C/50 % RH.

Starting the analysis of the curves obtained under negative *in-service* temperature conditions of pristine samples (*dry 0.00 wt %*) – Fig. 3a, there is a small shift on the Paris curve towards higher SERR values (7 %) compared to pristine sample (*dry 0.00 wt %*) tested at room conditions. In addition, low temperature showed a steepening of the slope (n) of the Paris curve, indicating a more pronounced sensitivity of the crack growth rate to variations in $\Delta\sqrt{G}$ or higher propagation growth rate. The reference slope for *dry 0.00 wt %* is 16.53, which was changed to 21.82 for the *dry 0.00 wt %* sample tested at −40 °C. In other words, there is a 32 % increase in slope. This trend suggests that low temperatures stiffen the matrix, decreasing its toughness and favouring a more brittle fracture [35].

It is worth noting that environmental conditioning affects both Paris parameters. Although the discussion here highlights the variation in the slope n, this inherently implies a corresponding adjustment in the constant C, since the two parameters are interdependent in shaping the curve. Therefore, changes in n reflect not only the altered propagation behaviour but also the overall shift in the fatigue crack growth kinetics due to hygrothermal effects.

Considering the high *in-service* temperature effect, a similar trend was observed when applying high temperature and different RH conditions during the test without precondition in a hygrothermal chamber. As the fatigue test time was not long enough to cause water absorption, the three curves at high temperature (80 °C) and different RH showed the same superimposed Paris curve (Fig. 3b).The strain energy release rate levels of the Paris regime remained essentially unchanged, indicating no reduction in the strength to opening delamination, in agreement with the results reported in Ref. [21]. However, a reduction in the slope was observed from 16.53 ± 0.42 for pristine sample (*dry 0.00 wt %*) to 14.49 ± 0.41, i.e. 12 % of reduction. This reduction at elevated temperatures is consistent with findings in the literature and has been associated with increased matrix ductility and increase in toughness of the matrix [36].

Regarding the effect of hygrothermal preconditioning, results present in Fig. 3c represent the pristine sample compared with those exposed in hygrothermal climatic chamber until reach the maximum equilibrium moisture content (*wet 1.20 wt %*). Both experiments presented in Fig. 3c were tested at room conditions (22°/50 % RH). The SERR range remains the same, following the found in the literature [16], but we can see a reduction of 13 % in the slope of Paris curve. This evidences a higher deformation behaviour before the fracture, characteristic of a tougher material [36]. Based on the similar change in the Paris parameters, temperature affects the Paris curve in a similar trend to preconditioned samples, although the mechanisms responsible for the modifications are different, as will be explained later.

Some authors [17,25] argue that no significant differences in the Paris curve are observed when hygrothermal preconditioning or *in-service* temperature are analysed individually, due to the limited experimental variation. This difference between the present results and the literature can be attributed to the implementation of an *in-service* climatic chamber control surrounding the fatigue machine, which provides more precise control of temperature and especially relative humidity during the test. Another factor that affects the comparison is the data processing methodology. For instance, using an alternative method to fit the da/dN curve (e.g. the 7-point method) may increase the apparent variability inherent in each test. In the present work, even for tests conducted at room conditions, temperature and relative humidity were tightly controlled, ensuring greater accuracy and reliability in the assessment of *in-service* hygrothermal effect. The reduction in slope may be associated with changes in fracture toughness behaviour due to matrix plasticisation or fibre-matrix interface degradation, both commonly induced by hygrothermal exposure.

When analysing the curves combining hygrothermal preconditioning and negative *in-service* temperature conditions (*wet 1.20 wt % at -40°C*) – Fig. 3d, there is a higher change in the Paris curve behaviour. The shift in the Paris curve in now towards higher SERR values, with an increase of 29 % for the wet (1.20 wt %) conditions compared to the reference curve (*dry 0.00 wt % at 22°C/50 %*). This trend suggests that crack propagation is more dependent on energy variations due to increased matrix embrittlement at low temperatures [35]. On the other hand, the slope of Paris curve (16.53 for the reference sample *dry 0.00 wt %*) slightly change to 17.02, showing a 3 % of increase. At this stage, the negative temperature resulted in a shift in the fatigue curve to higher $\Delta\sqrt{G}$ values and small increase in the slope, indicating an increased resistance to crack growth. This may be due to the combination of low temperature and wet condition, which increased matrix stiffness and a reduced the plasticity mechanisms. This behaviour is based on the changing of the hardness and fracture toughness of the material [37,38], while simultaneously increasing the growth rate once a critical threshold is exceeded. Two hypotheses have been proposed to explain this behaviour:

- Firstly, the absorbed moisture within the polymer matrix may partially crystallise under sub-ambient conditions, forming ice-like structures that behave similarly to micro-fillers [39]. These rigid inclusions could reinforce the crack tip region locally, thereby increasing the energy required for crack propagation.

- Secondly, the reduction in molecular mobility at low temperatures [40,41], which is further constrained by the presence of frozen moisture, may result in a stiffening effect that delays crack growth under cyclic loading.

While both hypotheses are consistent with the observed trend, further investigation is needed to confirm the underlying mechanisms and their contribution to fatigue resistance.

Considering the high *in-service* temperature test combined with preconditioning, there is an overlap of the curve for all three cases of EMC with similar Paris coefficients. The *wet (1.20 wt %) at 80°C/90 % RH*, *wet (0.85 wt %) at 80°C/50 % RH* and the *wet (0.55 wt %) at 80°C/30 % RH* presented the same range of SERR and exponents of 13.49, 13.26 and 13.98, respectively. This suggests that EMC causes irreversible damage in fatigue delamination, since saturating and then drying the specimen gives the same behaviour as for the saturated specimen and does not significantly alter the Paris curve. To evaluate the effect of combined moisture and temperature, the response of the preconditioned specimen (*wet 1.20 wt% at 80°C/90 % RH*) was compared to that of the pristine specimen (*dry 0.00 wt % at 22°C/50 % RH*) – Fig. 3e. The combined effect of preconditioning with high *in-service* temperature showed a shift in the SERR curve with an 32 % reduction in $\Delta\sqrt{G}$ and 18 % reduction of slope. This change in slope is attributed to the plasticisation of the matrix due to temperature and EMC, which causes the matrix to change its behaviour from brittle to more ductile as it starts to deform plastically before fracture [42]. Linear elastic fracture mechanics (LEFM)-based calculations remain valid, since the plasticisation is local and does not indicate global yielding [13,14]. The reduction in SERR ($\Delta\sqrt{G}$) may be associated to degradation of cohesive (breaking of polymer chains) and adhesive (fibre/matrix interface) and/or stiffness reduction, generated by excessive softening of the matrix.

This combined effect of hygrothermal preconditioning and low/high *in-service* temperature results in a more pronounced change in the Paris curve than both parameters applied in isolation. Notably, while most studies in the literature tend to investigate these environmental factors independently, the present results highlight the importance of considering their synergistic interaction, which may otherwise underestimate the extent of degradation observed under realistic service conditions.

A comparative analysis of Fig. 3 curves shows that preconditioning increases the change in delamination behaviour when combined with *in-service* temperature, a trend that is consistently observed for both low (Fig. 3d) and high temperature conditions (Fig. 3e). However, the direction of this effect is different. The combination of hygrothermal preconditioning with high temperature results in a reduction of $\Delta\sqrt{G}$ and a decrease in the slope. The combination with low temperature results in an increase in $\Delta\sqrt{G}$ and a rise in the slope. This opposite trend underlines the complex interaction between environmental conditions and temperature and highlights the need for combined assessments to fully capture material behaviour in service.

3.2. Thermo-mechanical interpretation of fatigue behaviour

Dynamic Mechanical Thermal Analysis (DMTA) results are presented in Fig. 4 to compare the viscoelastic behaviour of pristine (*dry 0.00 wt%*) and preconditioned samples (*wet 1.20 wt%*). The curves presented correspond to the representative curve, since both repetition curves were repeatable. In addition, samples that were preconditioned and then dried were also analysed, i.e., wet 0.55 wt%. Here, E' represents the elastic (or stored) modulus component, while tan (δ), defined as the ratio between the loss modulus (E'') and the storage modulus (E'), reflects the damping behaviour of the material. The storage modulus was affected by preconditioning and moisture uptake, showing a reduction of 9.1 MPa for the *wet 1.20 wt%* sample and 4.8 MPa for the *wet 0.55 wt%* sample, compared with *dry 0.00 wt%*.

Tan (δ) was used to identify the glass transition temperature (T_g), defined as the peak of these curves. The pristine specimens (*dry 0.00 wt %*) exhibited a single, well-defined peak in the tan δ curve, which is characteristic of thermoset matrices reinforced with continuous fibres. In contrast, the preconditioned specimens (*wet 1.20 wt%*) displayed a bimodal response, which is attributed to the heterogeneous plasticisation of the matrix. Water acts as a plasticiser, interacting preferentially with regions of the epoxy network that are less cross-linked or more polar, such as areas near the fibre or at defect sites [43,44]. This results in two distinct phases: one with a lower glass transition temperature (T_g) of ~173 °C, corresponding to plasticised, water-rich regions; and another with a higher T_g of 210–227 °C, representing areas less affected by moisture. This is not the result of a polymer blend, but rather a consequence of selective water absorption and localisation within the matrix. The effect of preconditioning and subsequent drying treatment is reflected in the DMTA curves, with partial recovery of the thermal behaviour (T_g).

A summary of the T_g values for dry and wet specimen after different environmental exposures indicates that hygrothermal preconditioning reduces the thermal stability of the composite, as evidenced by the

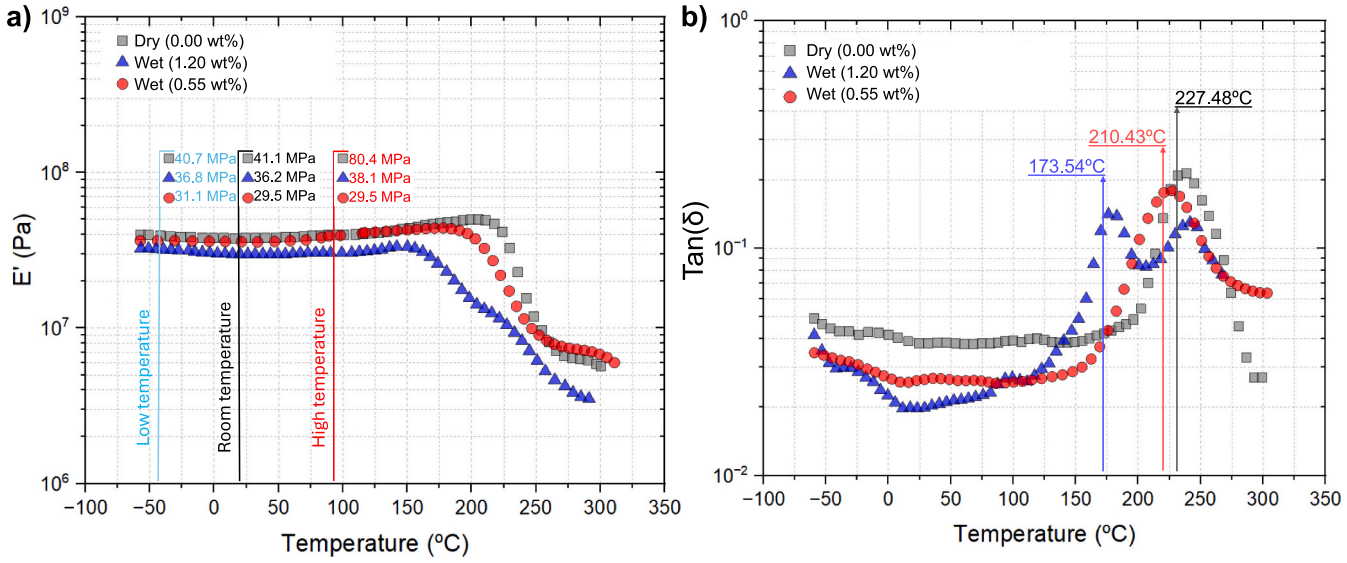

Fig. 4. DTMA curves: a) storage modulus (E') and b) Tan δ.

decrease in T_g. Flowing the work by Mamalis et al. [45], this reduction is primarily associated with moisture uptake and the resulting plasticisation of the polymer matrix. Specifically, T_g decreased from 227.48 °C (*dry 0.00 wt%*) to 173.54 °C for *wet 1.20 wt%* and partially recovered to 210.43 °C for the *wet 0.55 wt%*. A partial recovery of T_g was thus observed in the wet specimen after drying, as also reported in previous literature [16,17]. This behaviour is attributed to the partial desorption of moisture (see Fig. 1) and homogenization of cross-linking in a single phase. However, the incomplete water desorption results in the incomplete recovery. The moisture content might become a permanent block inside the material since the complete water desorption was not possible ever after a long exposure of high temperature and low RH. Also, polymer degradation processes, such as hydrolysis or chain scission, may also have contributed to the reduced T_g.

Although moisture desorption occurs during the drying process, this alone cannot fully explain the observed changes. When considered alongside the experimental evidence of incomplete recovery of thermal properties, it suggests that the polymer matrix and the fibre/matrix interface have undergone permanent degradation. Similar conclusion on material degradation was also made in literature [16,17]. These irreversible changes are probably responsible for long-term alterations to the material thermal and mechanical behaviour [25,45].

As illustrated in Fig. 5, the interaction between water molecules and the composite material occurs in multiple stages during preconditioning (see Fig. 1), in which stages A-D occurs during moisture absorption (Stage I-II in Fig. 1). In the initial stage (Stage A), it is presumed that the fibre/matrix interface remains intact, and water molecules are only present in the surrounding environment. In stage B, water begins to penetrate the composite, primarily diffusing through micro gaps and imperfections in the matrix to reach the fibre/matrix interface. At this stage, the water molecules are mainly in a free state and are not yet interacting strongly with the polymer chains [46]. In stage C, water molecules diffuse further into the matrix, where some are absorbed and become physically trapped between polymer chains. This can induce localised swelling and partial plasticisation of the matrix. Stage D is also referred to as the transformation stage, during which some of the absorbed water transitions into bound water. This transformation occurs through hydrogen bonding with polar groups in the polymer matrix or at the fibre/matrix interface [47]. Simultaneously, long-term exposure to high temperatures and humidity can cause the matrix to undergo thermal oxidative degradation or hydrolysis. This results in chain scission and the formation of additional polar sites that may interact further with water. Once saturation is reached, no further transformation of free water into bound water occurs and excess water or degraded by-products may diffuse out of the material [48]. The formation of new hydrogen bonds between matrix molecules and water (as bound water) can reduce the storage modulus, indicating a decrease in stiffness that can mitigate further environmental damage during cyclic loading. However, matrix degradation and the resulting reduction in the glass transition temperature (T_g) weaken interfacial adhesion and interlayer properties, significantly reducing fracture toughness [47].

Hobbiebrunken et al. [38] showed that the spatial distribution of von Mises stresses within fibre/matrix interface is influenced by temperature variations. At low temperatures (Fig. 6: $T < T_0$), molecular mobility is significantly restricted, resulting in increased hardness and brittleness. This restriction acts as a barrier to crack propagation, thereby increasing the energy required for damage propagation [38]. This behaviour reflects the increased brittleness of the material at low temperatures, where plasticity is reduced and fracture occurs more readily without significant plastic deformation [49]. In addition, low temperatures result in reduced crack stability and a more fragile interface.

Conversely, molecular mobility increases with high temperature (Fig. 6: $T > T_0$), leading to a reduction in stiffness and an increase in residual stresses [38,50]. This increased molecular mobility promotes plasticity of fracture behaviour, resulting in more stable crack propagation that is increasingly sensitive to variations in strain energy ($\Delta\sqrt{G}$) as reflected in the slope of the curve. Epoxy resin has a cross-linked molecular structure which inherently induces internal stresses that contribute to its dimensional stability. As temperature increases, molecular mobility tends to increase; however, the presence of cross-links limits significant molecular rearrangement, resulting in the development of internal stresses within the material [38,51]. The residual stress generated by the high temperature is responsible for reducing the energy required for damage propagation, shifting the $\Delta\sqrt{G}$ curve to lower values.

The thermo-mechanical analysis provided valuable insights into the distinct molecular mechanisms by which temperature and moisture content influence the fatigue behaviour of CFRP laminates. Although

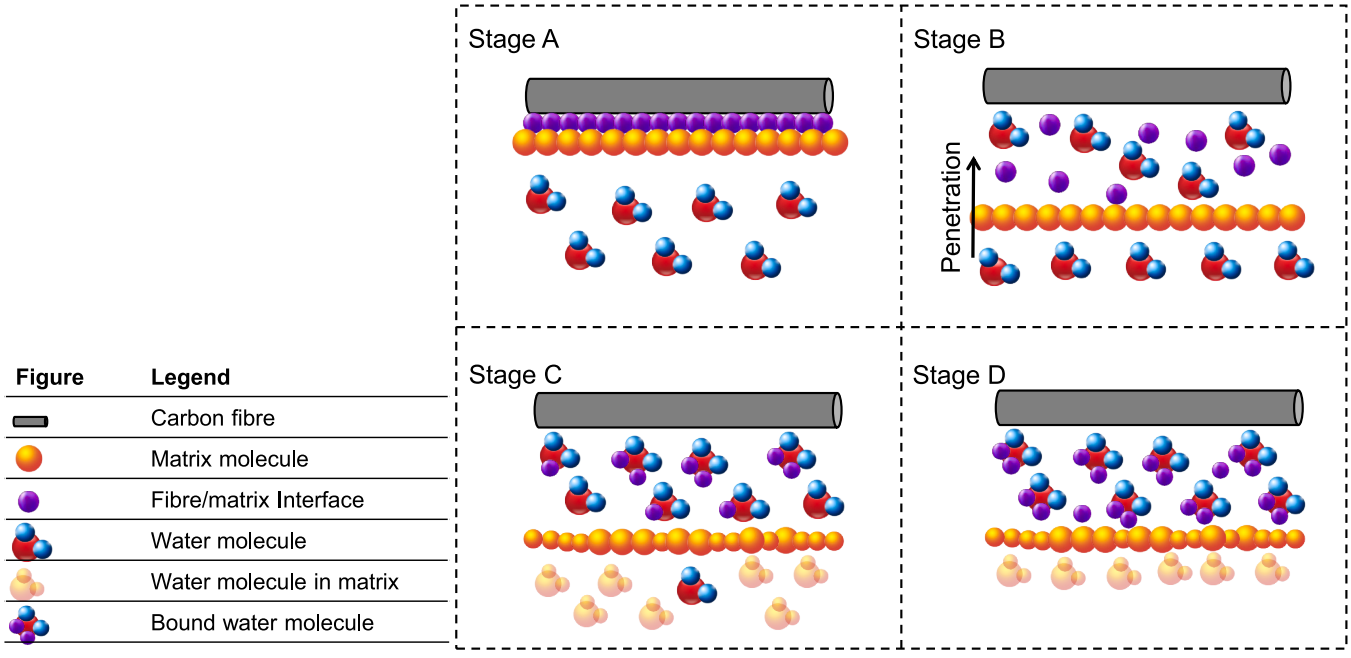

Fig. 5. Stages of moisture sorption in CFRP (adapted from Ref. [47]).

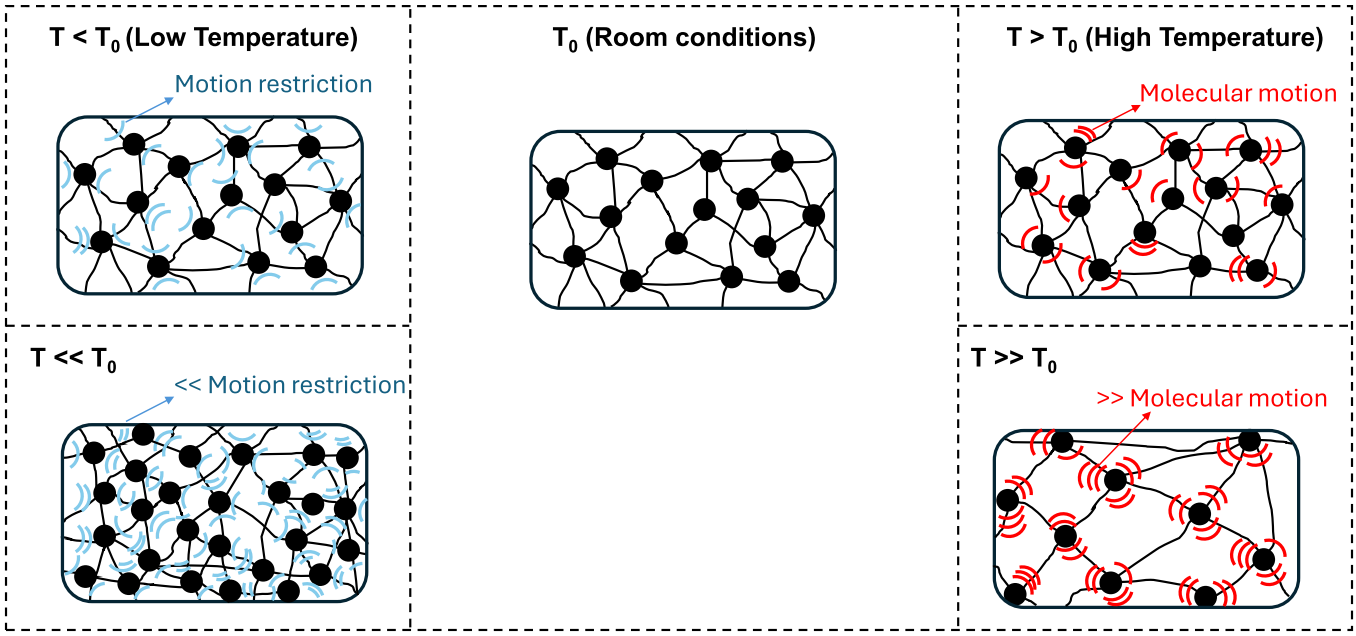

Fig. 6. Thermal effects on the spatial distribution of the epoxy molecular structure.

both factors independently resulted in similar macroscopic effects in the delamination behaviour, their underlying mechanisms are fundamentally different. Moisture uptake primarily promotes plasticisation of the matrix and interfacial weakening, whereas elevated temperature drives molecular mobility and softening. The simultaneous action of both conditions introduces a compounded effect, whereby distinct degradation mechanisms act concurrently, leading to more pronounced modifications in the Paris curve. These findings underscore the importance of characterising the coupled effects of environmental conditioning, rather than evaluating temperature and moisture effects in isolation, to achieve a more accurate understanding of the fatigue delamination resistance of composite laminates in real-world service environments.

3.3. Statistical analysis

All of the factors applied, i.e., equilibrium moisture content obtained during preconditioning and *in-service* environmental conditioning applied during fatigue testing, appear to influence the Paris curve under mode I fatigue delamination. In order to better understand the individual contribution of each factor, this section focuses on a statistical analysis of the Paris curve parameters. Table 3 shows the input factors, including the equilibrium moisture content – EMC (wt %) absorbed during preconditioning phase in climatic chambers prior to testing; the *in-service* temperature (°C) and relative humidity – RH (%) applied during fatigue testing. The Paris curve parameters were considered as response variables: $\Delta\sqrt{G_{ref}}$ at 5×10^{-7} m/cycle, which evaluates the shift in SERR, and the slope n of the curve. Table 3 summarises all the input factors and the responses obtained experimentally, considering the average of three replicates. The Paris parameters presented were obtained by fitting the experimental data to the Paris law equation (Eq. (3)), which relates the fatigue crack growth rate (da/dN) to the strain energy release rate (SERR) range. Specifically, the fitting was performed on the linear region of the Paris curve.

The analysis of variance (ANOVA) approach was applied to evaluate the variance in the Paris parameters and to assess the individual effects of environmental conditions applied before and during the fatigue tests. A single-factor analysis with repeated measures was conducted to compare the influence of different parameters on the response, using Minitab, following procedures outlined in references [52,53] and detailed in Appendix B. To better interpret the variability in the results, an ANOVA analysis was performed using the *F-test* method to assess the differences within the same material and between different hygrothermal conditions.

In ANOVA, the *F-value* represents the ratio of between-group variance, variation attributed to different input parameter conditions – preconditioning or in-situ environment conditions, and within-group variance (variation under the same condition). The $F_{critical}$ value works as a threshold for testing the null hypothesis (H_0), indicating whether a

Table 3
Environmental effects as input factors, and Paris parameters as response variables.

Hygrothermal preconditioning[a] (climatic chamber)	*in-service* environmental conditions[b] (during fatigue test)		Paris parameters (post-processed data)	
EMC	Temperature (°C)	Relative humidity (%)	$\Delta\sqrt{G_{th}}$ [N/m] (at 5×10^{-7} m/cycle)	Slope – *n*
Dry (0.00 wt%)	−40	–	101.23 ± 2.28	21.35 ± 1.12
Dry (0.00 wt%)	22	50	110.09 ± 7.53	16.67 ± 0.42
Dry (0.00 wt%)	80	90[c]	101.30 ± 2.83	16.17 ± 0.65
Dry (0.00 wt%)	80	50[c]	97.30 ± 5.12	16.42 ± 0.55
Dry (0.00 wt%)	80	30[c]	99.30 ± 2.14	16.77 ± 0.44
Wet (1.20 wt%)	−40	–	125.21 ± 1.33	17.45 ± 1.18
Wet (1.20 wt%)	22	50	99.23 ± 12.56	14.03 ± 0.41
Wet (1.20 wt%)	80	90	75.88 ± 3.68	13.31 ± 0.77
Wet (0.85 wt%)	80	50	75.38 ± 3.24	13.26 ± 1.01
Wet (0.55 wt%)	80	30	79.74 ± 2.05	13.31 ± 1.61

[a] – preconditioning in static climatic chambers (before the test).
[b] – conditioning during the fatigue test.
[c] RH was only applied for statistical purposes, since the exposure time was insufficient there was no change in moisture content.

given parameter has significant effect on the response. If *F-value* > $F_{critical}$, the null hypothesis is rejected, indicating that the factor has a significant effect on the response variable. In addition, *p-value* analysis was performed to ensure the statistical significance of the results. A *p-value* < 0.05 indicates that the confidence level for determining whether a factor affects the variability of the system is at least 95 %, confirming the reliability of the statistical conclusions. Finally, the percentage contribution (PC) of each factor was calculated to quantify its relative influence. This was determined as the ratio of the factor sum of squares (SS) to the total sum of squares (TSS), expressed as PC=(SS/TSS) × 100. The resulting PC value represents the proportion of the total variation in the response variable that can be attributed to a given factor [52,53].

EMC has the highest *F-value* (Table 4), followed sequentially by *in-service* temperature and relative humidity (applied during the test), in that sequence. The same sequential trend is observed in the percentage of contribution (PC) of each factor to the shift in $\Delta\sqrt{G_{ref}}$ values, EMC accounts for 50.68 %, test temperature for 9.02 %, and *in-service* RH for 7.99 %. However, the error (32.32 %) exceeds the contribution of the two last factors. This high error indicates some degree of insensitivity when evaluating the change in SERR, likely due to concurrent changes in the slope of the Paris curve, which alters the values of $\Delta\sqrt{G_{ref}}$ for a given crack growth rate (da/dN).

A *p-value* < 0.05 for EMC confirms its significant contribution to the variability of $\Delta\sqrt{G_{ref}}$. Similarly, test temperature shows a reliable influence with a *p-value* below the 0.05 threshold. In contrast, the higher *p-value* (>0.05) observed for *in-service* relative humidity indicates that this factor is statistically unreliable as the error associated with it exceeds its contribution (Table 4). Therefore, *in-service* temperature and RH applied during fatigue test could be considered as secondary factors in the relative change of $\Delta\sqrt{G_{ref}}$ in the Paris curve.

Similarly, Table 5 presents the ANOVA results for the slope of the Paris curve, taking into account the same factors of EMC (from the hygrothermal preconditioning), *in-service* temperature and relative humidity (from the *in-service* environmental conditions during the fatigue test).

A similar trend is observed for *in-service* RH, which has a *p-value* of 0.870 (>0.05), an *F-value* of 0.15 (< $F_{critical}$ = 2.58), and a small percentage contribution (less than the associated error). These results support the null hypothesis validity, indicating that relative humidity does not significantly affect the response. This result is expected since the relative humidity applied during fatigue test was primarily used to maintain the moisture content level induced by preconditioning and does not cause any additional changes in the material behaviour or in the Paris curve such as SERR shifts, or slope variations.

On the other hand, when analysing the effects of EMC (due to preconditioning) and *in-service* temperature (during the fatigue test), both factors show *F-values* significantly higher than $F_{critical}$, along with high percentage contributions. This confirms that in both cases the null hypothesis is invalid, and EMC and *in-service* temperature strongly influence the slope of the Paris curve. This conclusion is further validated by *p-values* < 0.05 and low associated error values, providing a high level of statistical confidence (95 %) in the observed trends.

However, considering that EMC is the primary factor influencing the SERR shift, while *in-service* temperature applied during fatigue test has the most significant effect on the slope of the Paris curve, it can be concluded that both parameters are key contributors to the observed degradation mechanisms. The EMC introduced during hygrothermal preconditioning mainly affects the energy required for crack propagation, whereas the *in-service* temperature during fatigue testing mainly determines the sensitivity of the crack growth rate, as reflected in the slope (*n*) of the Paris curve. Therefore, the combined effect of preconditioning and high/low *in-service* temperature leads to more pronounced changes in the Paris curve. In contrast, *in-service* relative humidity during the test did not cause any significant changes in the results and is considered mainly a control parameter to preserve the EMC established during the hygrothermal preconditioning phase, throughout the fatigue test.

Table 4
ANOVA for the change in SERR ($\Delta\sqrt{G_{ref}}$) of the Paris curve as response.

Factor/Parameter	SS[a]	MS[a]	*p-value*	$F_{critical}$	*F-value*	*PC*[a]
EMC (wt%)	2250.20	750.10	0.026	2.86	1.57	50.68 %
In-service temperature (°C)	267.10	133.50	0.021	2.86	0.28	9.02 %
In-service RH (%)	236.50	118.20	0.774	2.86	0.25	7.99 %
error	956.70	478.30	–	–	–	32.32 %

[a] SS – Sum of square; MS – Mean Square; PC – Percentage of contribution.

Table 5
ANOVA analysis for the change in slope (*n*) of the Paris curve as response variable.

Factor/Parameter	SS[a]	MS[a]	*p-value*	$F_{critical}$	*F value*	*PC*[a]
EMC (wt%)	11.32	5.66	0.035	2.58	2.97	25.61 %
In-service temperature (°C)	28.48	14.24	0.012	2.58	7.47	64.46 %
In-service RH (%)	0.57	0.29	0.870	2.58	0.15	1.29 %
error	3.81	1.91	–	–	–	8.63 %

[a] SS – Sum of square; MS – Mean Square; PC – Percentage of contribution.

3.4. Modelling environmental effects

Given the results presented earlier, where moisture content from hygrothermal preconditioning and the temperature applied during fatigue testing were identified as the most significant factors influencing the Mode I fatigue curve, both parameters are used in this section to model the Paris curve. The relative humidity applied during mechanical testing is neglected from this section, as it does not have a significant direct effect on the Paris parameters and acts mainly as a secondary factor to maintain the moisture absorbed during preconditioning. The aim of this section is to predict the environmental effects on the Paris curve using the empirical quadratic model described in Equation (5). This model enables interpolation of the behaviour of both the energy release rate threshold $\Delta\sqrt{G_{ref}}$ and the Paris curve slope *n*. The advantage of this model is the possibility of analysing the effects of equilibrium moisture content from preconditioning and temperature individually by setting either parameter, equilibrium moisture content (*EMC*) or the normalised $(T-T_g)/T_g$ to zero. Additionally, in the model a combined term is present to take into account the combined effects of both parameters. This analysis is reflected by the fitting parameters β, where the sign indicates direct/inverse proportionality of the linear (β_i or β_j), quadratic (β_{ii} or β_{jj}) and/or combined (β_{ij}) relation.

$$Z_i = Z_{0,i} + \beta_i(EMC) + \beta_j\left(\frac{T-T_g}{T_g}\right) + \beta_{ii}(EMC)^2 + \beta_{jj}\left(\frac{T-T_g}{T_g}\right)^2 + \beta_{ij}(EMC)\left(\frac{T-T_g}{T_g}\right) \quad (5)$$

Where, Z_i represents the parameter to be analysed ($i = \Delta\sqrt{G_{ref}}$, *n*), $Z_{0,i}$ is initial value of Z_i (based on reference conditions of temperature and EMC), *T* is the *in-service* temperature (*K*), T_g is the glass transition temperature (*K*), *EMC* is the equilibrium moisture content (wt%), and β denotes the fitting constants.

$(T-T_g)/T_g$ represents the normalised temperature, which is used to measure the relative deviation of the temperature applied during fatigue, based on the glass transition temperature (T_g). This term indicates how the material behaviour changes as the applied temperature deviates from T_g. At temperatures above (or close to) T_g, the epoxy matrix tends to have greater molecular mobility, resulting in enhanced plasticity. This typically lead to a decrease in $\Delta\sqrt{G_{ref}}$ and in the Paris curve slope.

On the other side, at temperatures well below T_g (i.e., the negative normalised temperature), the matrix becomes more rigid and brittle, leading to an increase of $\Delta\sqrt{G_{ref}}$ and of the Paris curve slope. *EMC* is the equilibrium moisture content absorbed during hygrothermal preconditioning, also normalised based on mass uptake. This parameter can increase the plasticity of the material, potentially mitigating the effects of increased stiffness at lower temperatures or amplifying plasticity at high temperature applied during the fatigue test. On the opposite side, moisture in sub-zero temperatures may turn to ice within the composite and that can also stiffen the matrix.

Fig. 7 illustrates the application of Equation (5) to the experimental data, resulting in interpolation curves with an $R^2 > 0.97$ for both cases. A second order polynomial relationship is observed between input parameters (temperature and EMC) the fitted Paris curve parameters ($\Delta\sqrt{G_{ref}}$ – Fig. 7a and n – Fig. 7b). The resulting three-dimensional models are described by Equations (6) and (7), corresponding to the respective plots shown in Fig. 7.

Equation (6) describes the parameter $\Delta\sqrt{G_{ref}}$, corresponding to a fixed crack growth rate (da/dN), as a function of temperature and EMC. The linear coefficient for EMC ($\beta_i = -92.58$) is negative, indicating that increasing absorbed moisture (m_c) leads to a decrease in $\Delta\sqrt{G_{ref}}$, i.e. less energy is required to propagate a delamination crack under fatigue. In contrast, the positive quadratic coefficient for EMC ($\beta_{ii} = 44.36$) suggests a non-linear trend where the rate of reduction in $\Delta\sqrt{G_{ref}}$ may slow or partially recover at higher moisture levels. Together, these coefficients reflect the softening and plasticisation of the matrix due to water uptake, which affects the resistance to crack propagation, particularly at intermediate EMC levels.

For the temperature dependent terms, the linear coefficient ($\beta_j = -219.93$) and the quadratic coefficient ($\beta_{jj} = -248.16$) are both negative. This indicates that as the temperature increases relative to the glass transition temperature (i.e. increasing $(T\text{-}T_g)/T_g$), there is a progressive decrease in $\Delta\sqrt{G_{ref}}$. This behaviour suggests thermal softening near or above the glass transition temperature, where the matrix loses stiffness and becomes more ductile, thereby reducing the ability of the material to resist delamination growth. The quadratic term further confirms that this reduction in $\Delta\sqrt{G_{ref}}$ increases at higher relative temperatures. It is important to note that more negative values of $(T\text{-}T_g)/T_g$ correspond to temperatures well below T_g, while values approaching zero or becoming positive indicate conditions closer to or above T_g, where thermal softening and increased molecular mobility lead to a greater susceptibility to delamination growth.

The interaction term ($\beta_{ij} = -114.17$) is also negative, indicating a synergistic degradation effect when both high temperature and high EMC are present. This suggests that while moderate increases in temperature or moisture alone may lead to a limited reduction in $\Delta\sqrt{G_{ref}}$, their combined effect amplifies the degradation mechanisms, such as matrix plasticisation and fibre-matrix interface weakening, resulting in a more severe reduction in delamination resistance.

Overall, the fitted surface captures the complex interplay between EMC and temperature, with a high degree of accuracy ($R^2 > 0.97$). This confirms that both parameters are critical in governing the fatigue delamination behaviour considering hygrothermal preconditioning and temperature conditions applied during the test.

$$\Delta\sqrt{G_{ref}}(T, EMC) = 57.09 - 92.58(EMC) - 219.93\left(\frac{T-T_g}{T_g}\right) + 44.36(EMC)^2 - 248.16\left(\frac{T-T_g}{T_g}\right)^2 - 114.17(EMC)\left(\frac{T-T_g}{T_g}\right) \quad (6)$$

$$n(T, EMC) = 19.91 + 0.42\,(EMC) + 29.52\left(\frac{T-T_g}{T_g}\right) + 0.42(EMC)^2 + 71.82\left(\frac{T-T_g}{T_g}\right)^2 + 5.45(EMC)\left(\frac{T-T_g}{T_g}\right) \quad (7)$$

The values presented in Equation (7) describe the variation of the Paris curve slope (n) as a function of EMC and temperature. The linear coefficient for EMC ($\beta_i = 0.42$) is positive, indicating that increasing absorbed moisture slightly increases the slope of the Paris curve. The same value is observed for the quadratic coefficient ($\beta_{ii} = 0.42$), suggesting a slight but consistent trend in which higher moisture levels slightly increase the sensitivity of the crack growth rate to $\Delta\sqrt{G_{ref}}$. This behaviour contrasts with the typical matrix plasticisation effect, suggesting that moisture alone plays a secondary role in controlling the slope, as found in ANOVA analysis.

Although both variables were normalised, it is important to note that the influence of each term in the polynomial model depends on the magnitude of the respective coefficients (β) but also on the actual variation intervals of the variables. In this case, the normalised temperature term $(T - T_g)/T_g$ ranges from −0.55 to 0.2, while the EMC varies from 0.00 to 1.20 wt%. Nevertheless, the fitted temperature-related coefficients are significantly larger, suggesting that temperature has a stronger influence within the explored experimental domain. However, caution should be taken when comparing the effects of variables with

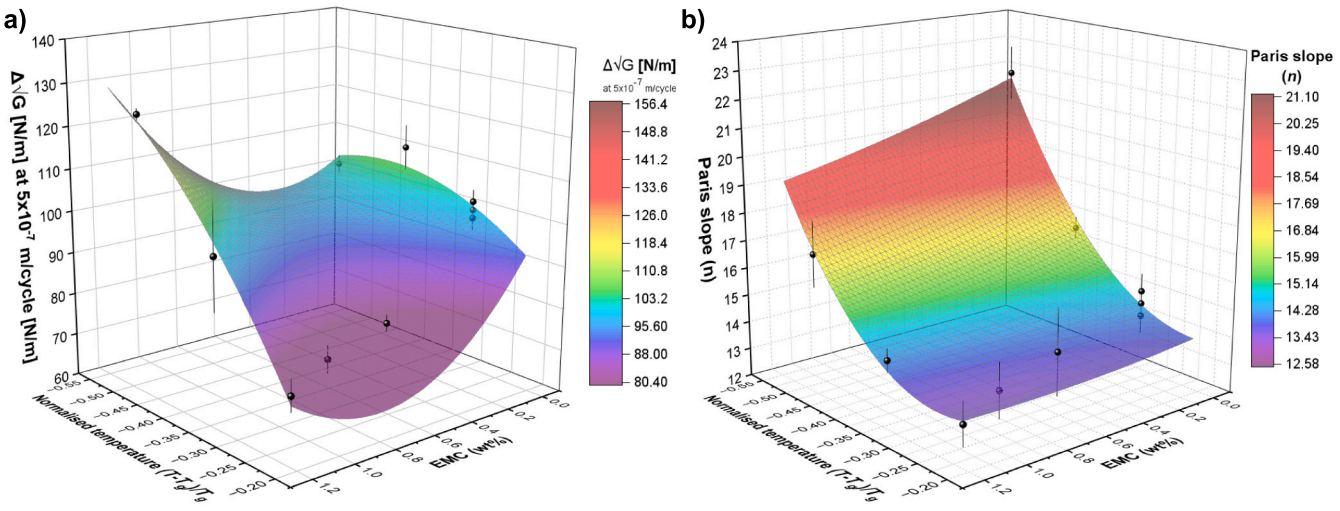

Fig. 7. Empirical interpolation of a) $\Delta\sqrt{G_{ref}}$ at 5×10^{-7} m/cycle and b) slope of Paris curve, depending on the EMC and normalised temperature.

different ranges and physical units.

Both coefficients (β_j and β_{jj}) for temperature range are positive. This suggests that near or above T_g, the matrix exhibits increased ductility, activating energy dissipation mechanisms. As a result, although the crack growth rate becomes less sensitive to small changes in energy release rate (i.e., reduced Paris slope), the dissipation mechanisms significantly modify the effective SERR values throughout fatigue propagation.

The interaction term ($\beta_{ij} = 5.45$) is also positive, implying that the combined presence of elevated moisture and temperature can further amplify the change in the slope *n*. This synergy contrasts with the behaviour observed for $\Delta\sqrt{G}$, where the interaction term led to degradation. Here the combined effect results in an increased slope, which may be related to changes in the fracture process zone, enhanced fibre bridging dynamics or matrix viscoelasticity under fatigue loading at elevated temperatures and humid conditions.

Using the simulated values of the shift in $\Delta\sqrt{G_{ref}}$ and the slope *n* as a function of temperature and EMC, it is possible to validate the proposed model curve against the experimental data using Equation (8). In this equation, *n* is a function of *T* and *EMC*, while *C* is also taken into account by considering the equivalence of the $\Delta\sqrt{G_{ref}}$ values found at 5×10^{-7} m/cycle, i.e. $C = C(T, EMC) = 10^{-7}/\left[\Delta\sqrt{G_{ref}}(T, EMC)\right]^{n(T,EMC)}$.

$$\frac{da}{dN} = C(T, EMC) \cdot \left[\Delta\sqrt{G}\right]^{n(T,EMC)} \tag{8}$$

Fig. 8 shows the experimental data points, while the lines represent the simulated values using Equation (8). For presentation purposes, only selected samples showing the most significant shifts in Paris curve are presented, including *Dry (0.00 wt%) at 22°C*, *Dry (0.00 wt%) at -40°C* (0.00 wt%), *Wet (1.20 wt%) at 22°C*, *Wet (1.20 wt%) at 80°C* and *Wet (1.20 wt%) at -40°C*. A strong correlation between the experimental and simulated data can be observed, with minimal deviation. This is further supported by Table 6, which compares the fitting errors between the experimental Paris parameters (Equation (3)) and the proposed model (Equation (8)).

The highest error recorded was 2.97 % for the slope of the Paris curve and 4.12 % for the change in SERR values, indicating that the proposed method is a reliable interpolation of the effects of hygrothermal preconditioning and *in-service* temperature conditions during mode I fatigue testing.

3.5. Fractographic analysis

Fig. 9 shows the optically measured height maps of fracture surfaces of specimens conditioned and tested under each condition previously presented. In all images, the crack propagation direction (da/dN) is from left to right. A comparative analysis between pristine (*dry 0.00 wt%*) and hygrothermally preconditioned samples (*wet 1.20 wt%*) revealed a significant increase in fibre bridging formation, as shown by the presence of loose fibres on the fracture surface shown in Fig. 9a (labelled A). Similarly, an increase in fibre bridging can be observed when transitioning from low to high *in-service* temperatures applied during fatigue testing. Besides the change in fracture toughness and stiffness induced by temperature and moisture content in CFRP, the combination of hygrothermal preconditioning and high *in-service* temperature promotes a densification of fibre bridging [54], which in turn plays a significant role in altering the Paris curve [55].

Based on Equation (4), fracture surface roughness was measured using high magnification images, as shown for each condition in Fig. 9b. The primary objective of this analysis was to quantify the intrinsic roughness of the fracture surface. To ensure accuracy, the analysis was carried out in a manner that excluded loose fibres resulting from fibre bridging, as their presence could influence the true roughness values.

To obtain a representative roughness profile, six sets of five parallel profile lines were analysed, with 4 pixels spacing between lines within the same set, providing 240 measurements for each condition. A comprehensive roughness profile was then generated, and roughness values were determined using Equation (4) (Fig. 10a). Eight images were taken for each specimen under each environmental condition (Fig. 10a).

Roughness was measured along profile lines oriented parallel to the fibre direction and aligned with the direction of crack propagation. This approach was adopted to minimise the influence of inherent surface roughness variations due to the nesting effect, an intrinsic characteristic of unidirectional (UD) composites. As hygrothermal preconditioning and in-service temperature primarily affect the polymer matrix phase, the main fractographic features are found in the resin-rich regions between the fibres. Therefore, the roughness measurements reflect an apparent transition from more ductile fracture behaviour, characterised by greater deformation prior to failure, to more brittle fracture behaviour, characterised by limited deformation and less dense fracture mechanisms. The surface height profile (Fig. 10a) obtained along each scan line can be integrated to yield a surface roughness value that

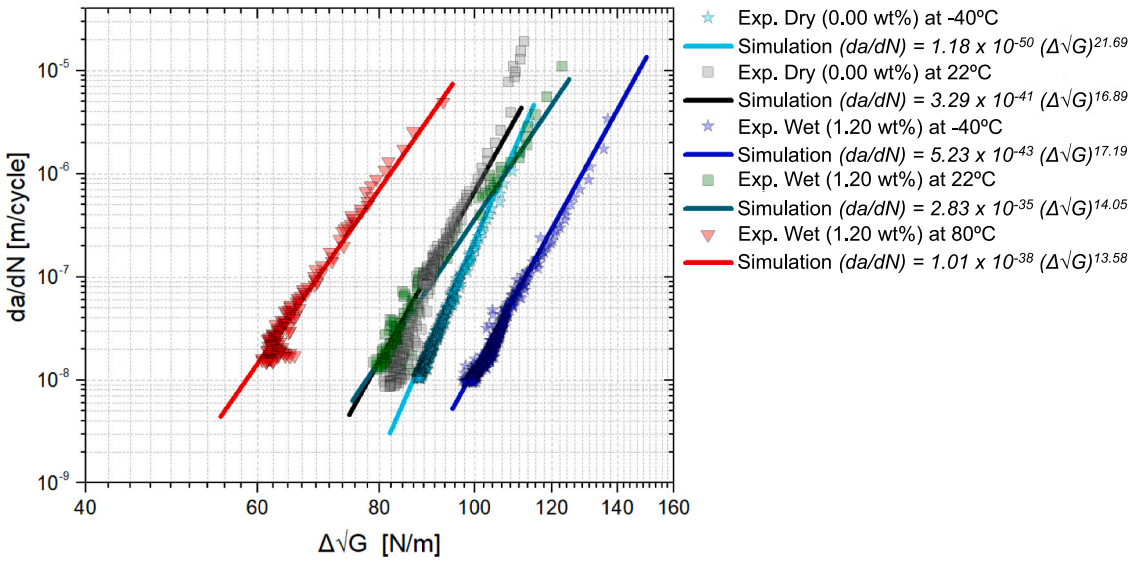

Fig. 8. Proposed empirical model applied to experimental data in the boundary environmental conditions.

Table 6
Comparative analysis between experimental and simulated Paris fitting of slope (n) and $\Delta\sqrt{G_{ref}}$ (at 5×10^{-7} m/cycle).

Environmental test conditions		Exp. Paris fit		Simulation fit			
EMC	*in-service* temperature (°C)	n	$\Delta\sqrt{G_{ref}}$ [N/m]	n	*error* (%)	$\Delta\sqrt{G_{ref}}$ [N/m]	*error* (%)
Dry (0.00 wt%)	−40	21.82	101.23	21.63	0.83	103.75	−2.49
Dry (0.00 wt%)	22	16.53	110.09	16.89	−2.22	110.09	4.12
Dry (0.00 wt%)	80	14.49	97.30	14.44	−2.97	97.30	−3.12
Wet (1.20 wt%)	−40	17.02	125.21	17.19	−1.02	123.79	1.14
Wet (1.20 wt%)	22	14.42	99.23	14.05	2.56	102.40	−3.20
Wet (1.20 wt%)	80	13.26	75.38	13.58	−2.46	77.89	−3.33

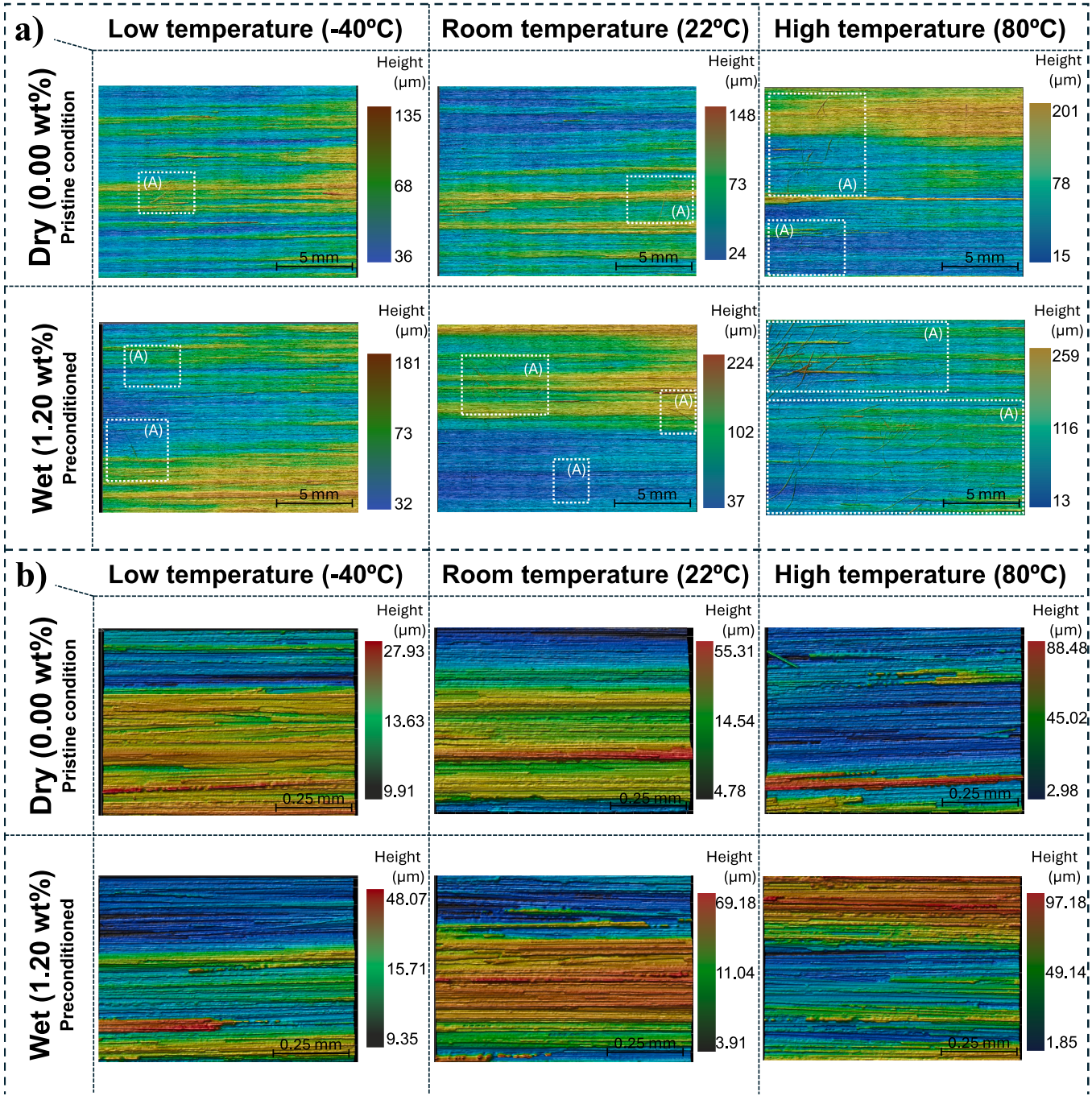

Fig. 9. Optical fractographic images highlighting the different combination of hygrothermal preconditioning (dry or wet) and *in-service* temperature conditions showing a) the presence of fibre bridging and b) the fracture surface roughness.

correlates directly with the prevailing fracture behaviour. This indicates a tendency towards either brittleness or ductility depending on the

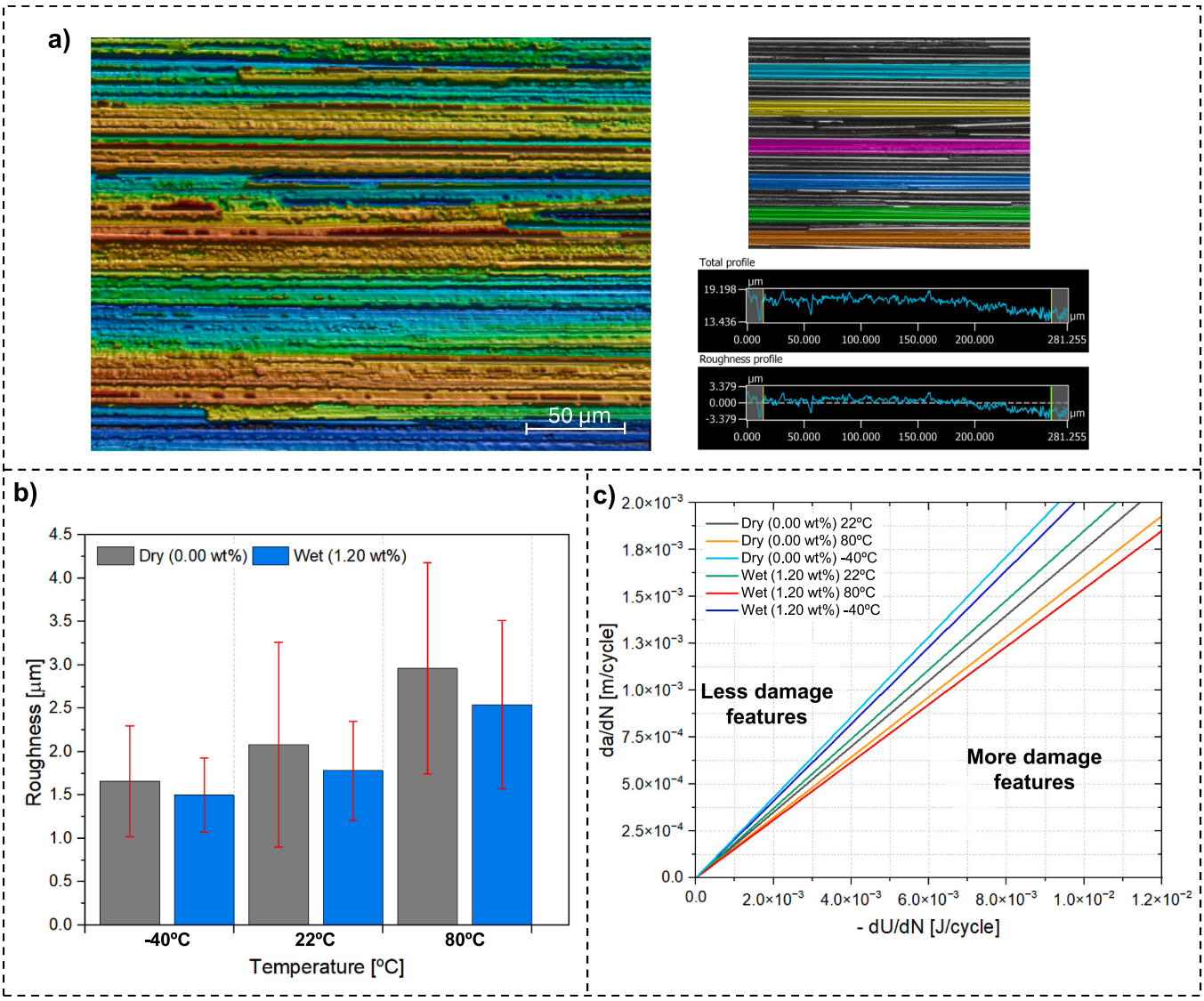

Fig. 10. Quantitative fracture analysis using optical microscopy: a) roughness profile measurement approach, b) surface roughness values under various conditions, c) energy release rate per cycle (-dU/dN) *vs crack growth rate* (da/dN) curve.

environmental conditions.

Fig. 10b shows the mean and standard deviation of the roughness measurements per specimen. Despite the relatively high standard deviation, a clear trend can be observed from the average perspective, in which the specimens tested at low temperatures showed the lowest roughness values, followed by an increase in roughness for those tested at room temperature and reaching its highest levels at high temperatures. Regarding the effect of preconditioning, *wet 1.20 wt%* specimens showed a lower roughness trend across all temperature conditions compared to *dry 0.00 wt%*, but less statistical significance.

Notably, this variation trend in surface roughness behaviour does not follow the same trend observed for the shift in strain energy release rate (SERR) in the Paris curve. However, it exhibits a pattern consistent with the variations found in the slope values of the Paris curves. A lower strain energy requirement per unit crack growth was observed at sub-zero temperatures, resulting in a less rough surface associated with fewer damage features. In contrast, at high temperatures, there is a decrease in the slope, implying a higher strain energy requirement per crack unit, and then higher roughness.

Applying the dU/dN model [56] (described in Appendix C), enables evaluation of the energy dissipated per unit crack growth (da/dN), which aligns well with the fracture surface roughness trends observed in Fig. 10c [57,58]. The different slopes in the da/dN *vs.* dU/dN curve suggest that the energy dissipation per cycle follows a trend similar to the slope (*n*) of the Paris curve. The higher slope in the dU/dN against da/dN is associated with greater propagation tortuosity (greater surface roughness) due to more damage features.

The roughness behaviour appears to correlate more strongly with the slope of the Paris curve and dU/dN than with the absolute SERR values. This is because dU/dN, which represents the energy dissipated per cycle, shows a similar trend to the slope of the Paris curve. Thus, the environmental factors (temperature and EMC) primarily influence the dissipation mechanisms active during a fatigue cycle, rather than the total strain energy release rate. While $\Delta\sqrt{G_{ref}}$ represents the fracture energy threshold, it does not necessarily reflect the local energy dissipation occurring during crack propagation, which is influenced by the roughness of the fracture surface and crack path tortuosity induced under different environmental conditions.

Fig. 11 shows the SEM fractographic images corresponding to each test condition, covering high to low temperature, dry 0.00 wt% and wet 1.20 wt% preconditioned samples. Fig. 11a shows fractographic images at low magnification, providing an overview of the global fracture morphology. Fig. 11b shows fracture details at higher magnification, highlighting local damage features. The direction of crack propagation

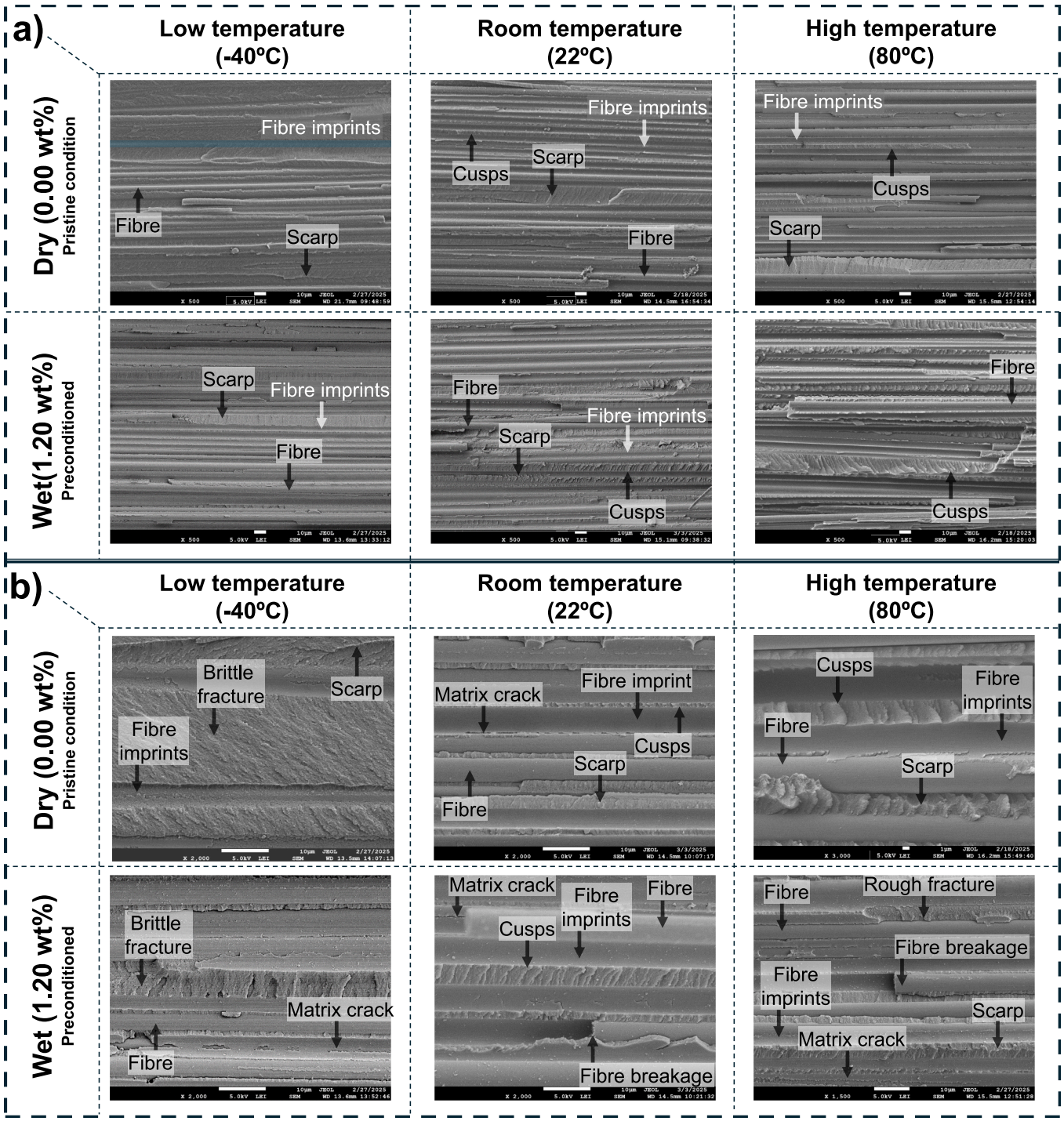

Fig. 11. SEM images highlighting the combination effect of hygrothermal preconditioning (dry or wet) and *in-service* temperature on fracture morphology a) low magnification (500X), b) higher magnification (>1.5 kX).

(da/dN) is consistently from left to right in all images, ensuring consistent interpretation of the observed fracture characteristics.

These SEM images confirm the findings of the optical microscopy analysis and provide further insight into specific underlying failure mechanisms. Key damage features associated with Mode I fatigue delamination such as cusps, scarps, fibre imprints, fibre breakage and matrix cracking are clearly visible. However, there is significant variation in the prominence and extent of these features as a function of *in-service* temperature and hygrothermal preconditioning states. The most pronounced morphological changes are predominantly observed within the matrix-rich zones, reflecting the high sensitivity of the epoxy matrix phase to environmental conditioning effects [23].

Fibre morphologies and imprints typically exhibited smooth surface characteristics, suggesting low interfacial adhesion between fibre and matrix. Cohesive failures, on the other hand, often exhibited well-defined cusp patterns resulting from local shear deformation during crack growth. These cusps, characterised by stepped or layered fracture surfaces are typically indicative of rapid fracture events with minimal associated plastic deformation, indicative of a brittle fracture.

At high temperatures, the fracture patterns become more pronounced, exhibiting a wavy and more expansive morphology. This indicates greater deformation before the fracture, consistent with more ductile fracture behaviour. Conversely, at low temperatures, the fracture patterns show less pronounced deformation, highlighting brittle fracture characteristics, as evidenced by the appearance of loose matrix granules. Brittle fracture occurs with minimal plastic deformation, primarily due to the increased material stiffness and reduced plastic deformation and ductility at lower temperatures [59,60].

Hygrothermal preconditioning increases deformation behaviour of fracture patterns at all temperature levels. As previously discussed, moisture uptake in the composite intensifies the deformation effects, through combined mechanisms such as plasticisation, swelling, and hydrolysis promoting ductile fracture behaviour marked by pronounced plastic deformation. In addition, an increased incidence of matrix cracking was observed in preconditioned specimens at all temperature levels, further indicating a weakening of the cohesive properties at the fibre-matrix interface.

The fracture behaviour observed in Fig. 11 can be compared to previous results from the literature [24]. In particular, Yao et al. [24] showed that elevated temperatures can promote fibre/matrix interface degradation, as indicated by the increased presence of fibre imprints in both dry and preconditioned specimens tested at 80 °C. This suggests fibre pull-out due to interfacial weakening. Conversely, at −40 °C, the interface is likely strengthened, as also reported in Ref. [24], leading to more matrix-dominated failure such as brittle fracture and matrix cracking, instead of fibre pull-out. This reflects a shift in the dominant failure mechanism from interfacial to cohesive failure in the matrix. Therefore, the SEM results corroborate the temperature-dependent interfacial effects previously described and reinforce the link between hygrothermal conditions and the underlying fracture mechanisms in fatigue delamination.

4. Conclusions

This study investigated the individual and combined effect of hygrothermal preconditioning and *in-service* temperature and relative humidity conditions on Mode I fatigue delamination in carbon fibre-reinforced polymer (CFRP) laminates. A comprehensive experimental campaign was conducted combining fatigue testing at different *in-service* temperatures and relative humidity levels, dynamic mechanical thermal analysis (DMTA), fractographic analysis, statistical modelling and empirical interpolation.

The results show that the EMC absorbed during hygrothermal preconditioning and *in-service* temperature are the main factors affecting the slope (n) of the Paris curve. These two parameters act synergistically to significantly alter the fatigue crack growth behaviour. In contrast, the *in-service* relative humidity presented no statistical effect and mainly acts to maintain the EMC established during the hygrothermal preconditioning stage.

Low temperature conditions increased material brittleness and resistance to fatigue crack growth, shifting the Paris curve to higher slope (n). Conversely, high temperatures promoted matrix plasticisation, flattening the Paris curve slope. The combination of hygrothermal preconditioning with either extreme *in-service* temperature condition enhanced these effects, adding the shift of the curve for high (hot-wet condition) or lower (cold-wet condition) SERR values. As a matter of fact, this result highlights the synergistic impact of environmental degradation on fatigue delamination behaviour, specially evaluated by preconditioning and *in-service* environment application during fatigue testing.

An empirical model was proposed to describe the combined effects of EMC and *in-service* temperature on the Paris curve parameters. The model demonstrated excellent correlation with the experimental data ($R^2 > 0.97$), allowing reliable prediction of environmental degradation trends under operational conditions.

Fractographic analysis corroborated these findings, by linking changes in fibre bridging, surface roughness, and energy dissipation mechanisms to the observed shifts in fatigue behaviour. Overall, this study is unprecedented and highlights the importance of considering both preconditioning and *in-service* environmental effects when assessing the long-term durability of composite structures.

CRediT authorship contribution statement

Francisco Maciel Monticeli: Writing – original draft, Visualization, Methodology, Investigation, Formal analysis, Data curation, Conceptualization. **Davide Biagini:** Writing – review & editing, Validation, Formal analysis, Data curation. **John-Alan Pascoe:** Writing – review & editing, Supervision, Resources, Project administration, Funding acquisition. **Yasmine Mosleh:** Writing – review & editing, Supervision, Project administration, Funding acquisition, Conceptualization.

Declaration of competing interest

The authors disclose to have no financial and personal relationships with other people or organizations that could inappropriately influence their work.

Acknowledgements

The research was funded by the European Union under GA No. 101091409 (D-STANDART). Views and opinions expressed are however those of the author(s) only and do not necessarily reflect those of the European Union. Neither the European Union nor the granting authority can be held responsible for them.

Appendix A

Figure A1 shows experimental data points and fitting of the Paris curve for each condition. The labels describe the preconditioning (including the equilibrium moisture content) and the temperature and relative humidity applied during the fatigue test.

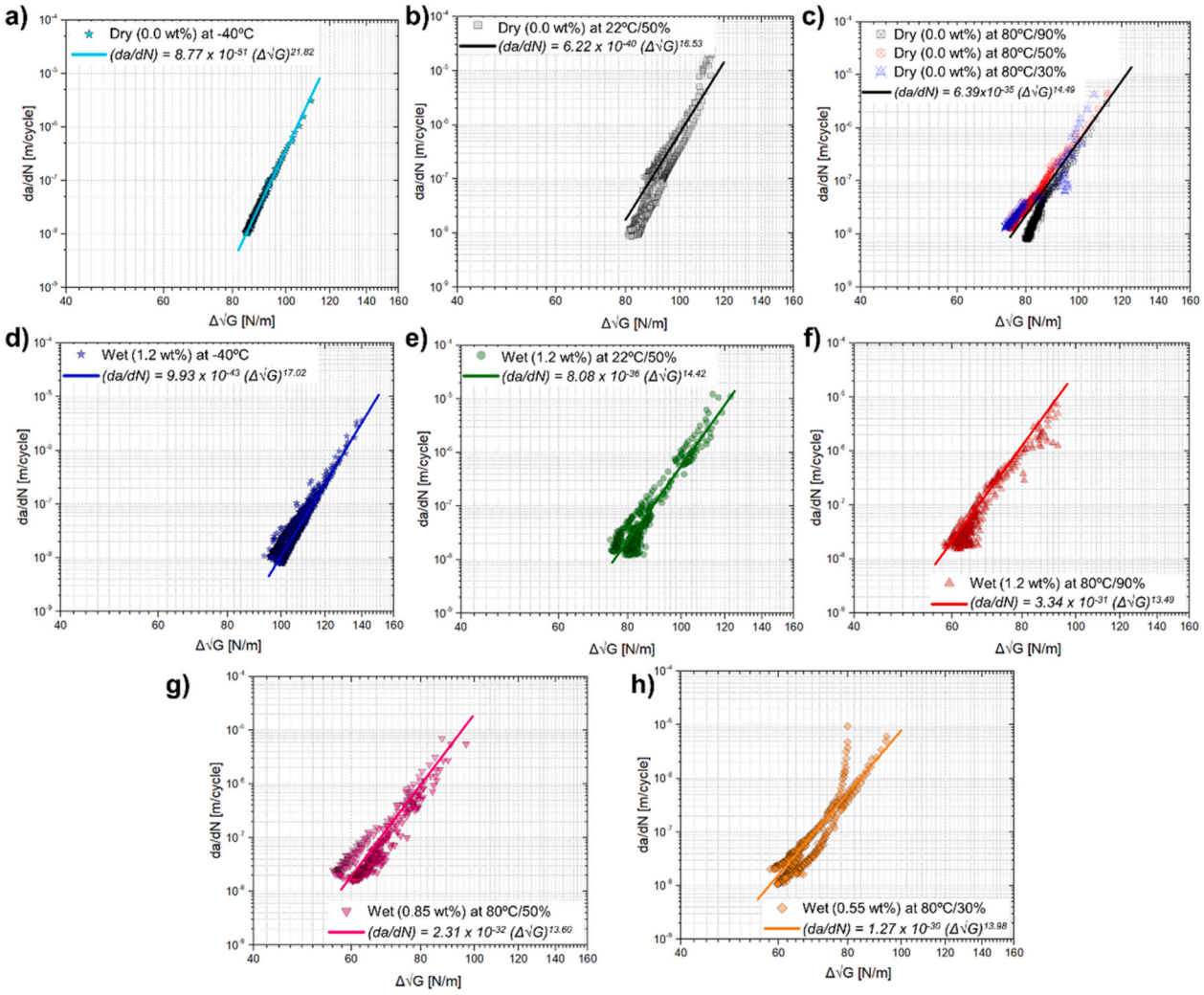

Fig. A1. Paris curve for each condition: a) Pristine (−40 °C), b) Pristine (22 °C/50 %), c) Pristine (80 °C/30–90 %), d) HA (−40 °C), e) HA (22 °C/50 %), f) HA (80 °C/90 %), g) HA (80 °C/50 %), h) HA (80 °C/50 %).

Appendix B

For the statistical analysis described in Section 3.2, *F value*, $F_{critical}$ and *p-value* were calculated using the software MiniTab18. To determine if the difference between a current value and the mean is significant, the p-value could be compared with its level of significance (α) to assess the null hypothesis. A significance level $\alpha = 0.05$ is generally used, which denotes the probability of the null hypothesis being valid as 5 %.

We can then distinguish two cases:

(1) *F value* > $F_{critical}$ and *p-value* ≤ α: The differences between some of the averages are statistically significant. If the p-value is less than or equal to the significance level, one can reject the null hypothesis and conclude that all population averages are not equal.

(2) *F value* < $F_{critical}$ and *p-value* > α: The differences between some of the averages are not statistically significant. In this case, it is not possible to reject the null hypothesis, as there is insufficient evidence to conclude that the group means differ. Therefore, it cannot be concluded that the population means are significantly different.

Table B1 shows the equations used for initial calculation of sum of square, degrees of freedom, square of means and F factor.

Table B1
Structure and equations for ANOVA

Variation	Sum of squares (SS)	Degree of freedom	Square of means (SM)	*F value*
Factor	$S_a = \sum_{i=1}^{C} n_s(\bar{x}_i - \bar{\bar{x}})^2$	$V_a = C_s - 1$	$SM_a = \frac{S_a}{V_a}$	$F = \frac{SM_a}{SM_b}$
Global	$S_b = \sum_{i=1}^{C} \sum_{j=1}^{n} (x_{ji} - \bar{x}_i)^2$	$V_b = n_s - V_b$	$SM_b = \frac{S_b}{V_b}$	

where, n_s is the number of experimental data, C_s the number of groups, $\bar{x}_i$ the average of each group, $\bar{\bar{x}}$ represents the total average, x_{ji} is the F value representing the analysis factor evaluated to determine if the global parameter variation is greater than the variability of observations for the parameter analysed.

Appendix C

The dU/dN method was calculated using force and the displacement to capture the strain energy in the specimen, following the equation bellow [56]:

$$\delta_0 = \delta_{min} - C_c P_{min} \tag{C1}$$

$$U_{mono} = \frac{1}{2} P_{min}(\delta_{min} - \delta_0) \tag{C2}$$

$$U_{cyc} = \frac{1}{2}(P_{max} - P_{min})(\delta_{max} - \delta_{min}) + P_{min}(\delta_{max} - \delta_{min}) \tag{C3}$$

$$U_{tot} = U_{mono} + U_{cyc} \tag{C4}$$

Where, P is the load, δ is the opening displacement, C_c is the compliance $[(\delta_{max} - \delta_{min})/(P_{max} - P_{min})]$, U_{tot} is the total strain energy in the system, U_{cyc} is the cyclic work which is applied during a load cycle, U_{mono} is the constant energy, and δ_0 is the displacement for which the force is 0.

Data availability

The data underlying this work is publicly available via a Zenodo repository: 10.5281/zenodo.15049770.

References

[1] Morioka K, Tomita Y, Takigawa K. High-temperature fracture properties of CFRP composite for aerospace applications. Mater Sci Eng, A 2001;319–321:675–8. https://doi.org/10.1016/S0921-5093(01)01000-0.

[2] Ravishankar B, Nayak SK, Kader MA. Hybrid composites for automotive applications – a review. J Reinforc Plast Compos 2019;38:835–45. https://doi.org/10.1177/0731684419849708.

[3] Alam P, Robert C, Ó Brádaigh CM. Tidal turbine blade composites - a review on the effects of hygrothermal aging on the properties of CFRP. Composites Part B 2018;149:248–59. https://doi.org/10.1016/j.compositesb.2018.05.003.

[4] Li X, Monticeli F, Pascoe JA, Mosleh Y. Interlaminar fracture behaviour of emerging laminated-pultruded CFRP plates for wind turbine blades. Eng Fract Mech 2024;308. https://doi.org/10.1016/j.engfracmech.2024.110353.

[5] Alabtah FG, Mahdi E, Eliyan FF. The use of fiber reinforced polymeric composites in pipelines: a review. Compos Struct 2021;276:114595. https://doi.org/10.1016/j.compstruct.2021.114595.

[6] He X, Ohsawa I, Takahashi J. Influence of marine and harsh environments on performance of carbon fiber paper reinforced polyamide 6. Fibers Polym 2021;22:3425–36. https://doi.org/10.1007/s12221-021-1465-0.

[7] Hamzat AK, Murad S, Adediran IA, Asmatulu E, Asmatulu R. Fiber - reinforced composites for aerospace , energy , and marine applications : an insight into failure mechanisms under chemical , thermal , oxidative , and mechanical load conditions. Adv Compos Hybrid Mater 2025;8:152. https://doi.org/10.1007/s42114-024-01192-y.

[8] Sethi S, Ray BC. Environmental effects on fibre reinforced polymeric composites: evolving reasons and remarks on interfacial strength and stability. Adv Colloid Interface Sci 2015;217:43–67. https://doi.org/10.1016/j.cis.2014.12.005.

[9] Li X, Zhang X, Chen J, Huang L, Lv Y. Effect of marine environment on the mechanical properties degradation and long-term creep failure of CFRP. Mater Today Commun 2022;31:103834. https://doi.org/10.1016/j.mtcomm.2022.103834.

[10] Al-Salloum YA, Almusallam TH. Creep effect on the behavior of concrete beams reinforced with GFRP bars subjected to different environments. Constr Build Mater 2007;21:1510–9. https://doi.org/10.1016/j.conbuildmat.2006.05.008.

[11] Ju J, Morgan RJ. Characterization of microcrack development in BMI-carbon fiber composite under stress and thermal cycling. J Compos Mater 2004;38:2007–24. https://doi.org/10.1177/0021998304044773.

[12] Ghasemi AR, Tabatabaeian A, Moradi M. Residual stress and failure analyses of polymer matrix composites considering thermal cycling and temperature effects based on classical laminate plate theory. J Compos Mater 2019;53:3021–32. https://doi.org/10.1177/0021998318812127.

[13] Jumahat A, Soutis C, Jones FR, Hodzic A. Fracture mechanisms and failure analysis of carbon fibre/toughened epoxy composites subjected to compressive loading. Compos Struct 2010;92:295–305. https://doi.org/10.1016/j.compstruct.2009.08.010.

[14] Banea MD, Da Silva LFM, Campilho RDSG. Effect of temperature on tensile strength and mode i fracture toughness of a high temperature epoxy adhesive. J Adhes Sci Technol 2012;26:939–53. https://doi.org/10.1163/156856111X593649.

[15] Dransfield K, Baillie C, Mai YW. Improving the delamination resistance of CFRP by stitching-a review. Compos Sci Technol 1994;50:305–17. https://doi.org/10.1016/0266-3538(94)90019-1.

[16] Yao L, He Z, He Y, Jin Q, Lomov SV, Alderliesten RC. Hygrothermal ageing effects on mode I fatigue delamination in multidirectional composite laminates. Int J Fatig 2024;188:108520. https://doi.org/10.1016/j.ijfatigue.2024.108520.

[17] Yao L, Wei J, He Z, He Y, Lomov SV, Alderliesten RC. Does hygrothermal degradation of mode I fatigue delamination resistance in carbon fibre reinforced polymer laminates depend on the ageing conditions? Compos Struct 2024;342:118240. https://doi.org/10.1016/j.compstruct.2024.118240.

[18] Deng J, Zhou J, Wu T, Liu Z, Wu Z. Review and assessment of fatigue delamination damage of laminated composite structures. Materials 2023;16. https://doi.org/10.3390/ma16247677.

[19] Morgado GF de M, Montagna LS, Gouvêa RF, Guimarães A, Passador FR, Rezende MC. Fatigue and durability assessment of PA6-based carbon fiber composites for lightweight applications. J Compos Mater 2023;57:4227–38. https://doi.org/10.1177/00219983231207148.

[20] Koumoulos EP, Trompeta AF, Santos RM, Martins M, Dos Santos CM, Iglesias V, et al. Research and development in carbon fibers and advanced high-performance composites supply chain in Europe: a roadmap for challenges and the industrial uptake. J Compos Sci 2019;3. https://doi.org/10.3390/jcs3030086.

[21] Arouche MM, Pavlovic M. Experimental and numerical analysis of the effect of temperature on the mode I and mode II delamination of glass fiber woven composites. Composites Part B 2025;293:112131. https://doi.org/10.1016/j.compositesb.2025.112131.

[22] Landry B, Laplante G, Leblanc LR. Environmental effects on mode II fatigue delamination growth in an aerospace grade carbon/epoxy composite. Compos Part A Appl Sci Manuf 2012;43:475–85. https://doi.org/10.1016/j.compositesa.2011.11.015.

[23] Charalambous G, Allegri G, Hallett SR. Temperature effects on mixed mode I/II delamination under quasi-static and fatigue loading of a carbon/epoxy composite. Compos Part A Appl Sci Manuf 2015;77:75–86. https://doi.org/10.1016/j.compositesa.2015.05.016.

[24] Yao L, Chuai M, Li H, Chen X, Quan D, Alderliesten RC, et al. Temperature effects on fatigue delamination behavior in thermoset composite laminates. Eng Fract Mech 2024;295:109799. https://doi.org/10.1016/j.engfracmech.2023.109799.

[25] Yao L, Wang J, He Y, Zhao X, Chen X, Liu J, et al. Hygrothermal effects on fatigue delamination behavior in composite laminates. Compos Struct 2024;330:117830. https://doi.org/10.1016/j.compstruct.2023.117830.

[26] Ramírez FMG, Garpelli FP, Sales R de CM, Cândido GM, Arbelo MA, Shiino MY, et al. Hygrothermal effects on the fatigue delamination growth onset in interlayer toughened CFRP joints. Int J Fatig 2020;138:105729. https://doi.org/10.1016/j.ijfatigue.2020.105729.

[27] Costa ML, Rezende MC, de Paiva JMF, Botelho EC. Structural carbon/epoxy prepregs properties comparison by thermal and rheological analyses. Polym Plast Technol Eng 2006;45:1143–53. https://doi.org/10.1080/03602550600887251.

[28] Zhang B, Ali H, Allegri G, Hallett SR. An experimental and numerical investigation into tensile fatigue failure of composite laminates containing wrinkles and cut plies. Int J Fatig 2025;198:109026. https://doi.org/10.1016/j.ijfatigue.2025.109026.

[29] Maurya A, Tanneru SP, Rajan S, Pereira JM, Miller SG. Experimental tests to characterize the behavior and properties of IM7-8552 composite. NASA/TM-20230001560; 2023, 20097.

[30] ASTM standard. Astm D 5229– 92 – Standard test method for moisture absorption properties and equilibrium conditioning of polymer matrix composite materials. Annu Book ASTM Stand 2010;92:1–13. https://doi.org/10.1520/D5229.
[31] Williams A, Hamerton I, Allegri G. Environmental effects of moisture and elevated temperatures on the mode I and mode II interlaminar fracture toughness of a toughened epoxy carbon fibre reinforced polymer. Polymers 2025;17. https://doi.org/10.3390/polym17111503.
[32] ASTM D5528. Standard test method for mode I interlaminar fracture toughness of unidirectional fiber-reinforced polymer matrix composites. Am Soc Test Mater 2021;1:1–14. https://doi.org/10.1520/D5528_D5528M-21.
[33] ASTM D6115. Standard test method for mode I fatigue delamination growth onset of unidirectional fiber-reinforced polymer matrix composites. Am Soc Test Mater 2019;1:1–7. https://doi.org/10.1520/D6115-97R19.
[34] Standard a. D5528-01 2001. Standard test method for mode I interlaminar fracture toughness of unidirectional fiber-reinforced polymer matrix composites. Am Soc Test Mater 2014:1–13. https://doi.org/10.1520/D5528-13.2.
[35] LeBlanc J, Cavallaro P, Torres J, Ponte D, Warner E, Saenger R, et al. Low temperature effects on the mechanical, fracture, and dynamic behavior of carbon and E-glass epoxy laminates. Int J Lightweight Mater Manuf 2020;3:344–56. https://doi.org/10.1016/j.ijlmm.2020.05.002.
[36] Charalambous G, Allegri G, Hallett SR. Temperature effects on mixed mode I/II delamination under quasi-static and fatigue loading of a carbon/epoxy composite. Compos Part A Appl Sci Manuf 2015;77:75–86. https://doi.org/10.1016/j.compositesa.2015.05.016.
[37] Hübner F, Brückner A, Dickhut T, Altstädt V, Rios de Anda A, Ruckdäschel H. Low temperature fatigue crack propagation in toughened epoxy resins aimed for filament winding of type V composite pressure vessels. Polym Test 2021;102. https://doi.org/10.1016/j.polymertesting.2021.107323.
[38] Hobbiebrunken T, Fiedler B, Hojo M, Ochiai S, Schulte K. Microscopic yielding of CF/epoxy composites and the effect on the formation of thermal residual stresses. Compos Sci Technol 2005;65:1626–35. https://doi.org/10.1016/j.compscitech.2005.02.003.
[39] Natarajan TS, Stöckelhuber KW, Malanin M, Eichhorn KJ, Formanek P, Reuter U, et al. Temperature-dependent reinforcement of hydrophilic rubber using ice crystals. ACS Omega 2017;2:363–71. https://doi.org/10.1021/acsomega.6b00443.
[40] Sethi S, Ray B. Mechanical behavior of polymer composites at cryogenic temperatures. Polym Cryog Temp 2013;1:61–108. https://doi.org/10.1007/978-3-642-35335-2.
[41] Sápi Z, Butler R. Properties of cryogenic and low temperature composite materials – a review. Cryogenics 2020;111:103190. https://doi.org/10.1016/j.cryogenics.2020.103190.
[42] Zafar A, Bertocco F, Schjødt-Thomsen J, Rauhe JC. Investigation of the long term effects of moisture on carbon fibre and epoxy matrix composites. Compos Sci Technol 2012;72:656–66. https://doi.org/10.1016/j.compscitech.2012.01.010.
[43] Gibhardt D, Buggisch C, Meyer D, Fiedler B. Hygrothermal aging history of amine-epoxy resins: effects on thermo-mechanical properties. Front Mater 2022;9:1–14. https://doi.org/10.3389/fmats.2022.826076.
[44] Shen W, Chen Y, Wang T, Huang Y, Li Z, Zhang W, et al. Study on hygrothermal aging of glass fiber/epoxy composites fabricated from dual-axis warp-knitted and flat-weave woven prepregs. Polym Compos 2025:1–10. https://doi.org/10.1002/pc.70015.
[45] Mamalis D, Floreani C, Ó Brádaigh CM. Influence of hygrothermal ageing on the mechanical properties of unidirectional carbon fibre reinforced powder epoxy composites. Composites Part B 2021;225:109281. https://doi.org/10.1016/j.compositesb.2021.109281.
[46] Chateauminois A, Vincent L, Chabert B, Soulier JP. Study of the interfacial degradation of a glass-epoxy composite during hygrothermal ageing using water diffusion measurements and dynamic mechanical thermal analysis. Polymer (Guildf) 1994;35:4766–74. https://doi.org/10.1016/0032-3861(94)90730-7.
[47] Zhang S, Hu J, Fang J, Xuan S, Zhou J, Tian W. Investigation on interlayer debonding behavior of unidirectional composite laminates under cyclical hygrothermal aging duration effects. Polym Compos 2024;45:6830–44. https://doi.org/10.1002/pc.28232.
[48] De'Nève B, Shanahan MER. Water absorption by an epoxy resin and its effect on the mechanical properties and infra-red spectra. Polymer (Guildf) 1993;34:5099–105. https://doi.org/10.1016/0032-3861(93)90254-8.
[49] Goncalves PT, Arteiro A, Rocha N. Experimental characterization and numerical analysis of CFRPs at cryogenic temperatures. Int J Mech Sci 2024;265:108899. https://doi.org/10.1016/j.ijmecsci.2023.108899.
[50] Reis AK dos, Monticelli FM, Neves RM, de Paula Santos LF, Botelho EC, Luiz Ornaghi Jr H. Creep behavior of polyetherimide semipreg and epoxy prepreg composites: structure vs. property relationship. J Compos Mater 2020;1:1–11. https://doi.org/10.1177/0021998320927774.
[51] Patil SU, Shah SP, Olaya M, Deshpande PP, Maiaru M, Odegard GM. Reactive molecular dynamics simulation of epoxy for the full cross-linking process. ACS Appl Polym Mater 2021;3:5788–97. https://doi.org/10.1021/acsapm.1c01024.
[52] Asiltürk I, Neşeli S, Ince MA. Optimisation of parameters affecting surface roughness of Co28Cr6Mo medical material during CNC lathe machining by using the Taguchi and RSM methods. Meas J Int Meas Confed 2016;78:120–8. https://doi.org/10.1016/j.measurement.2015.09.052.
[53] Monticeli FM, Almeida JrJHS, Neves RM, Ornaghi FG, Ornaghi HL. On the 3D void formation of hybrid carbon/glass fiber composite laminates : a statistical approach. Compos Part A Appl Sci Manuf 2020;137:106036. https://doi.org/10.1016/j.compositesa.2020.106036.
[54] Alessi S, Pitarresi G, Spadaro G. Effect of hydrothermal ageing on the thermal and delamination fracture behaviour of CFRP composites. Composites Part B 2014;67:145–53. https://doi.org/10.1016/j.compositesb.2014.06.006.
[55] Monticeli FM, Biagini D, Mosleh Y, Pascoe JA. A novel analytical model to characterise the monotonic and cyclic contribution of fibre bridging during mode I fatigue delamination in (C)FRPs. Composites Part B 2025;297:112319. https://doi.org/10.1016/j.compositesb.2025.112319.
[56] Pascoe JA, Alderliesten RC, Benedictus R. Characterising resistance to fatigue crack growth in adhesive bonds by measuring release of strain energy. Procedia Struct Integr 2016;2:80–7. https://doi.org/10.1016/j.prostr.2016.06.011.
[57] Mohammadi R, Najafabadi MA, Saghafi H, Saeedifar M, Zarouchas D. The effect of mode II fatigue crack growth rate on the fractographic features of CFRP composite laminates: an acoustic emission and scanning electron microscopy analysis. Eng Fract Mech 2021;241:107408. https://doi.org/10.1016/j.engfracmech.2020.107408.
[58] Amaral L, Yao L, Alderliesten R, Benedictus R. The relation between the strain energy release in fatigue and quasi-static crack growth. Eng Fract Mech 2015;145:86–97. https://doi.org/10.1016/j.engfracmech.2015.07.018.
[59] Coronado P, Argüelles A, Viña J, Mollón V, Viña I. Influence of temperature on a carbon-fibre epoxy composite subjected to static and fatigue loading under mode-I delamination. Int J Solid Struct 2012;49:2934–40. https://doi.org/10.1016/j.ijsolstr.2012.05.018.
[60] Argüelles A, Viña J, Canteli AF, Coronado P, Mollón V. Influence of temperature on the delamination process under mode i fracture and dynamic loading of two carbon-epoxy composites. Composites Part B 2015;68:207–14. https://doi.org/10.1016/j.compositesb.2014.08.051.